Investigation into the Effect of Plasmon Boosting of TiO_2 for Photocatalytic Destruction of Organic Molecules

Michael Ashton

MPhil **2013**

Investigation into the Effect of Plasmon Boosting of TiO_2 for Photocatalytic Destruction of Organic Molecules

Michael Ashton

A thesis submitted as partial fulfilment

Of the requirements of

Manchester Metropolitan University for the degree of Master of Philosophy

Department of Chemistry

Manchester Metropolitan University

Funding by EPSRC and United Utilities

May 2013

Contents

List of Figures

List of Tables

Commonly Used Abbreviations

SPR – Surface Plasmon Resonance

TiO_2 – Titanium Dioxide

APS – (3-aminopropyl)trimethoxysilane

TEOS - Tetraethylorthosilicate

RhB - Rhodamine B

SEM – Scanning Electron Microscope

TEM – Transmission Electron Microscope

PCS – Photon Correlation Spectroscopy

THPC - tetrakis(hydroxymethyl)phosphonium chloride

PVP – Polyvinylpyrrolidone 10,000

AU – Arbitrary Units

Abstract

Aim: To investigate the effect of gold nanoparticle surface plasmon resonance (SPR) on titanium dioxide (TiO_2) photocatalysis for the breakdown of organic molecules in different settings.

Experimental: Four types of nanoparticle were fabricated for this investigation; Silica-dye colloid (A), gold core silica-dye shell (B), silica-dye core coated in gold seeds (C), silica-dye core coated in a gold nanoshell (C). The dye used in this investigation was Rhodamine B isothiocyanate (RhB). The particles were used to examine their fluorescent boosting effects and therefore their potential at boosting photocatalytic activity. The particles were tested for fluorescence using the same amount of dye molecules and also underwent photocatalytic exposure with TiO_2 films produced by magnetron sputtering.

Results: Gold core silica-dye shell nanoparticles (B) gave almost five-fold enhancement. The silica-dye core coated in gold seeds (C) also boosted fluorescence enhancement by a factor of almost 200, a much greater increase compared to the gold core particle (B). TiO_2 enhances the photo-bleaching of RhB through a loss of fluorescence on its own, and a further doubling the rate when exposed to gold nanoparticles. When encapsulated in silica a protective barrier is formed preventing normal breakdown of dye, however, using a gold core or gold seeds on the nanoparticle surface overcame this barrier to degrade the dye by a small amount.

1.0 Introduction

Organic molecules are becoming an increasing problem for the drinking and waste water industry. Organic pollution originates from many different sources such as: agricultural, domestic, industrial and natural[1-4]. The European Parliament set up the Drinking Water Inspectorate in order to monitor and control levels of harmful substances within drinking water. As part of this they published a list of priority substances that are notably dangerous to environmental and human health should they persist at high levels within the water supply[5-6].

Table 1. European Union Priority Substance list of Organic Molecules[5].

Number	EU number	Name of priority substance	Source of contaminant
(1)	240-110-8	Alachlor	Herbicide
(2)	204-371-1	Anthracene	Combustion of fuel
(3)	217-617-8	Atrazine	Herbicide
(4)	200-753-7	Benzene	Constituent to crude oil and many aromatic hydrocarbons.
(5)	not applicable	Polybrominated diphenylethers	Building materials, electronics, furnishings, motor vehicles, airplanes, plastics, polyurethane foams and textiles.
(6)	287-476-5	Chloroalkanes	Polyvinylchloride (PVC) production, Pesticides, Insulation
(7)	207-432-0	Chlorfenvinphos	Insecticide and Acaricide.
(8)	220-864-4	Chlorpyrifos	Insecticide
(9)	203-458-1	1,2-Dichloroethane	PVC Production
(10)	200-838-9	Dichloromethane	Solvent for use in paint stripper, de greaser, decaffeinating coffee, aerosol propellant.
(11)	204-211-0	Bis(2-ethylhexyl)phthalate (DEHP)	Plasticiser in medical equipment, PVC, cosmetics and fragrences.
(12)	206-354-4	3-(3,4-dichlorophenyl)-1,1-dimethylurea	herbicide
(13)	204-079-4	Endosulfan	Insecticide
(14)	205-912-4	Fluoranthene	Combustion of fuel

Number	EU number2	Name of priority substance	Source of contaminant
(15)	204-273-9	Hexachlorobenzene	Fungicide
(16)	201-765-5	Hexachlorobutadiene	Solvent
(17)	210-168-9	Hexachlorocyclohexane	Pesticides
(18)	251-835-4	Isoproturon	Fungicide
(19)	202-049-5	Naphthalene	Chemical intermediate, Insecticide fumigant.
(20)	not applicable	Nonylphenols	Precursor to detergents
(21)	not applicable	Alkylphenols	Precursor to detergents, additive in fuel and lubricants, polymers, fragrances, antioxidants and fire retardant materials
(22)	210-172-0	Pentachlorobenzene	Manufacture of pesticides and fungicides
(23)	201-778-6	Pentachlorophenol	Herbicide, insecticide, pesticide, algaecide and disinfectant.
(24)	not applicable	Polyaromatic hydrocarbons(PAH)	Combustion of fuel
(25)	204-535-2	Simazine	Herbicide
(26)	not applicable	Tributyltin compounds	Biocides
(27)	234-413-4	Trichlorobenzenes	Precursor for dye and pesticides
(28)	200-663-8	Trichloromethane (chloroform)	Solvent, organic synthesis
(29)	216-428-8	Trifluralin	Herbicide
(30)	204-082-0	Dicofol	Precursor to pesticides
(31)	217-179-8	Perfluorooctane sulfonic acid and its derivatives (PFOS)	Textiles, paint, paper, polish, varnish, cleaning products, fire fighting foam
(32)	not applicable	Quinoxyfen	Fungicide
(33)	not applicable	Dioxins and dioxin-like compounds	By product of industry
(33)	277-704-1	Aclonifen	Pesticide
(35)	255-894-7	Bifenox	Herbicide
(36)	248-872-3	Cybutryne	Pesticide
(37)	257-842-9	Cypermethrin	Insecticide
(38)	200-547-7	Dichlorvos	Insecticide
(39)	not applicable	Hexabromocyclododecanes (HBCDD)	Flame retardent
(40)	200-962-3 / 213-831-0	Heptachlor and heptachlor epoxide	Insecticide
(41)	212-950-5	Terbutryn	Herbicide
(42)	200-342-2	17α-ethinylestradiol	Contraceptive pill
(43)	200-023-8 17	17β- estrodiol	Hormone treatment
(44)	239-346-4	Diclofenac	Anti-inflammatory drug

Naturally occurring organic pollutants degrade over time such as metabolisation by micro-organisms. The water industry takes advantage of this by using naturally occurring micro-organisms to remove dangerous molecules from waste water as they convert this to new bacteria cells, carbon dioxide and other byproducts[5]. This usually removes 90% of organic matter in waste water. Advanced biological treatment is also used to reduce levels of nitrate and phosphorus, which when introduced to the environment causes algae bloom, resulting in damaging the aquatic environment. Bacteria do this by converting nitrates into nitrogen gas or harmless nitrate and phosphorus into solids that can be later removed. The 10% of the remaining organic matter resisted biological breakdown due to their synthetic nature. The micro-organisms cannot therefore metabolise them. This organic matter consists of pesticides from agricultural use, organic waste products from industry and pharmaceuticals. These molecules are capable of causing significant environmental damage to organic life at high enough concentrations and could potentially come into contact with the drinking water supply and affect human health[7]. Polycyclic aromatic hydrocarbons (PAH) are seen as priority substances according to Table 1. These organic compounds compose of fused aromatic rings often found in fossil fuels. They are some of the key air pollutants found in built up, high population areas as by-products of fuel consumption. These pollutants dissolve in water when they are drained into the local natural environment or possibly used as drinking water after purification. PAH's vary in their toxicity dependant on their isomers making them non-toxic to extremely toxic. Benzo (a) pyrene is notably the first carcinogen to be discovered often found in cigarette smoke[8]. The study conducted by Gasperi et al (2008)[9] analysed the levels within Paris and its local waterways as part of the drinking water directive by the European parliament. They discovered that PAH's were present in all samples taken for testing during both dry and wet weather. According to the study the levels varies in frequency over different weather periods but not concentration. Benzo (a) pyrene showed an average concentration level of 0.06 μgL^{-1}, with a maximum of 0.24 μgl^{-1}, which could pose a risk to environmental and human health. These

pollutants can quite easily occur within the drinking water from rivers near areas of high population and industry. The Ter River near Barcelona reported high pollutant levels due to local industries and domestic areas, of which the river is the primary water source in that area[10]. Current water treatment technology does not deal with these organic waste products in drinking water or waste/sewage since they are not affected by naturally occurring micro-organisms normally used to remove them, nor do they break down naturally in the environment. They therefore persist in the natural environment, originally occurring at harmless levels, however further increase in the levels of these compounds is capable of causing damage to wildlife or being reintroduced into the drinking water supply and cause adverse effects to human health. New technologies are needed to tackle this issue.

This project aims to investigate the chemical property of titanium dioxide (TiO_2) photocatalysis films in conjunction with surface plasmon resonance boosting from gold nanoparticles to provide enhanced organic compound breakdown. This will be achieved by utilising cutting edge nanotechnology to maximise the SPR effect by producing different forms of nanoparticles. The TiO_2 photocatalysis and its effects will be measured by photobleaching of rhodamine B isothiocynate dye.

1.2 Current and New Technology

Current water treatment involves different processes depending on the contamination level of the water. There are two types, sewerage and wastewater. Sewerage (brown water) is waste originating from domestic areas, while other wastewater (grey water) may originate from industrial sites and could include additional pollutants that require separate treatment. All sewage and waste water is treated and then reintroduced into the environment[11]. 'NE water' in Singapore however is the only company to recycle wastewater directly into drinking water[12]. In the case of NE water they use high grade reclaimed water that undergoes further purification including micro filtration, removing any large particles and micro-organisms and reverse osmosis that allows only small molecules such as

water through leaving negligible organic concentration levels. Sewerage/waste water undergoes three treatment stages[10]. The primary stage involves separation of solid material by either settling or allowing oils and light material to float to the surface. These solids and oils are removed while the liquid moves on. Secondary treatment involves breakdown of organic matter by water borne micro-organisms, which naturally metabolise some of the organic matter as described before. An additional next step known as tertiary treatment is dependent upon the remaining contaminants within the water. This involves sterilization from the previous stage by chemicals or microfiltration. Additional specific bacteria may be used to remove contaminants such as nitrates and phosphorus. The tertiary stage may be vigorous using new and expensive technology, for example if the water was being reintroduced directly into to the water supply, or this might be very basic in areas where the water will enter a low risk environment.

Potable water is defined as water suitable for human consumption or with low long term risk. Most potable water undergoes 6 processes[13]. The first step is to screen the water for any large pieces of debris such as leaves or twigs. Smaller particles are then filtered out by auto-coagulation tanks specific mixture of coagulant chemical. Coagulated particles are then allowed to settle in clarification tanks and removed as sludge while the clear water is then chlorinated to disinfect and kill any bacteria that could be a danger to human health. Water is run through rapid gravity filters such as sand and gravel pits, often also including carbon to filter out some pesticides if required. The water undergoes a final chlorination check and additional chlorine is added if required. From this process, it is clear there are no widely used techniques for removing organic contaminants.

Currently water treatment is only effective at degrading organic molecules that micro-organisms are capable of metabolising leaving the majority of pharmaceuticals that are resistant to this breakdown. New technologies are being developed to meet the objectives set out by the water framework directive and the EU Parliament[5, 6]. Nanofiltration technologies are emerging as a possibility by having the potential to filter out pesticides, pharmaceuticals, microorganisms and metal salts[14]. Uncharged particles are filtered out by size exclusion, the pores of the membrane

being large enough for small molecules to pass through. Charged particles such as metal ions can also be filtered out according to the charge difference of the ion and the membrane surface. One method uses iron oxides to trap heavy metals. Sand is coated with the iron oxide which then is used as a filter. Heavy metals are attracted to the iron oxide and become trapped and isolated from the water. Smaller organic molecules with a molecular weight less than 100 can still easily pass through these systems. Organic molecules can be specifically filtered by active carbon, which attracts pollutants and holds them in the nanofilter structure, isolating it from the water[15]. Organic molecules are naturally attracted to activated carbon however the effectiveness of this filter decreases as the active carbon sights become blocked. The filter must therefore be regenerated before it can be used again. This process is expensive due to the filters being regularly regenerated and maintained, not to mention the initial cost of producing these filters.

A different practical approach to removing organic pollutants is destroying or denaturing them through chemical means. In order to break down such molecules, highly reactive chemicals such as hydrogen peroxide (H_2O_2) and UV light is required[16]. Such treatment can improve pollutant control by molecules breaking down to water and carbon dioxide or by coagulation thereby allowing easy removal through filtration. Ozone is also capable of oxidizing organic pollutants and destroying them. Pisarenko et al[17] reported that ozone could also help reduce levels of nitrosodimethylamine, which is created in the post chlorination step of the potable water treatment. By introducing H_2O_2 as well, the efficiency of organic removal is further increased. Chemical removal can also be achieved indirectly by photocatalysis of titanium dioxide (TiO_2)[18]. A TiO_2 film is irradiated with UV light initiating photocatalysis producing hydroxyl radicals by splitting water molecules and superoxide from the electron donation capable of reducing and oxidizing organic pollutants. The benefit of such a system is that there is no need to introduced chemicals to the water supply; however, electrical energy is required to power the UV lamp. Improvements to the technique have been studied such as using a TiO_2 film sensitive to visible light through doping[19, 20]. The process changes the TiO_2

properties to excite at visible wavelengths and potentially take advantage of the abundant (and free) sunlight opposed to powering a UV lamp.

1.3 Titanium Dioxide Photocatalysis

Titanium dioxide is a naturally occurring oxide of titanium (TiO_2). As a mineral, it occurs in three different forms, anatase, rutile and brookite[21]. There are many different methods of analysing TiO_2 films. For imaging TEM and SEM are used frequently providing a basic idea of the crystal structure and therefore some indication of the type of crystal produced. Examples are shown in Figure 1.

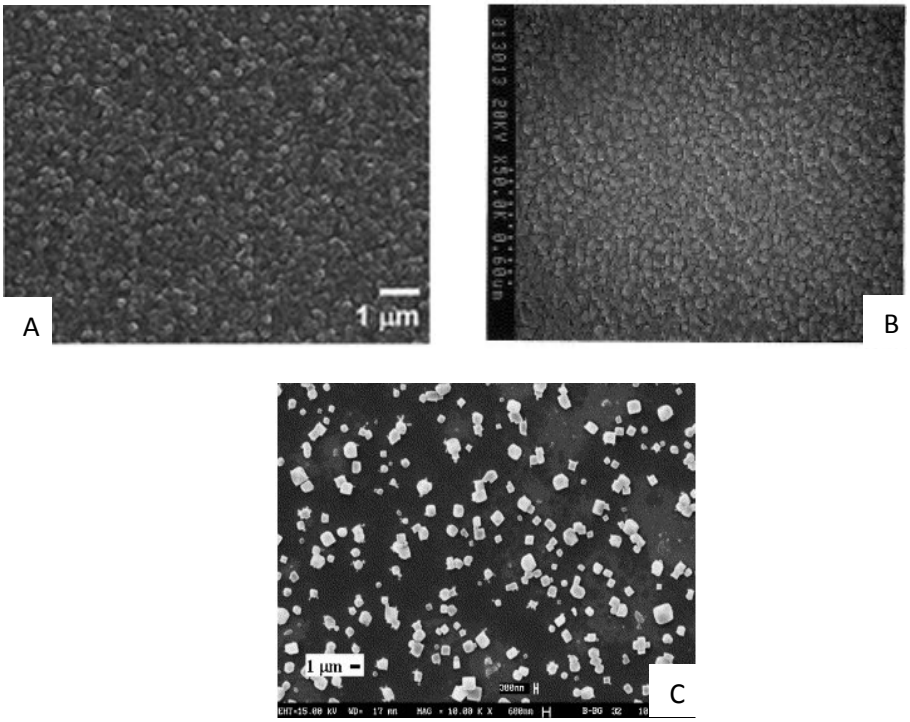

Figure 1. SEM images of titanium dioxide films for (A) anatase, (B) rutile, (C) brookite.

For a more accurate measurement of crystal formation X-ray diffraction and Raman Spectroscopy (shown in Figure 2), which are used to help identify and quantify the different crystals formed. This is important when predicting the possible properties the TiO_2 films possess.

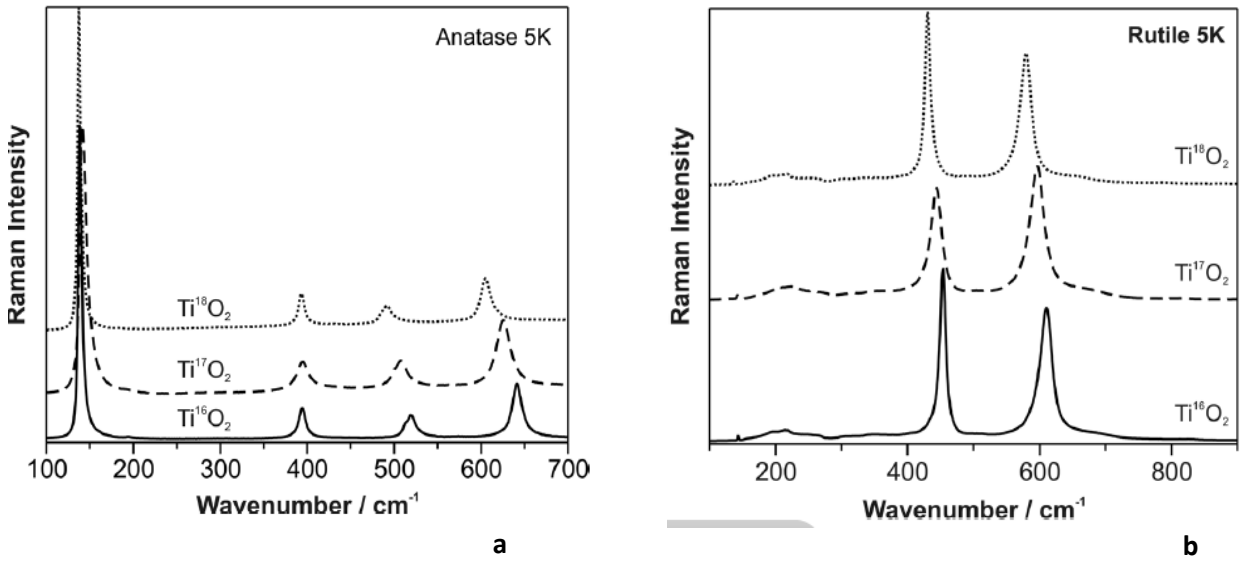

Figure 2. Raman Spectra of (a) anatase and (b) rutile.

TiO_2 possesses interesting properties including photocatalysis. This is the process involving TiO_2 using light energy, specifically UV light for pure TiO_2, to cause molecules to become charged producing electrons and positive holes[22]. These photogenerated charge carriers diffuse to the surface allowing them to interact with surface molecules such as water and oxygen. The positive holes can react with water molecules forming hydroxyl radicals, which can reduce organic molecules. Electrons also diffuse to the surface and can react with oxygen producing superoxide, oxidising organic molecules.

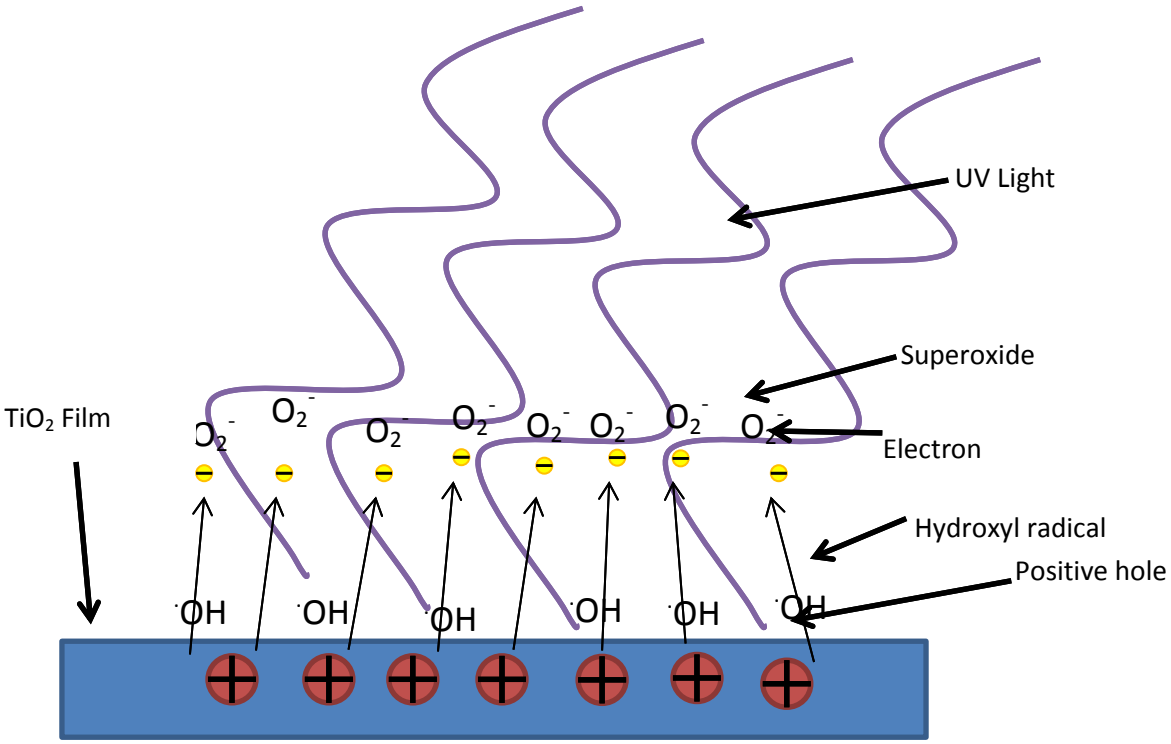

Figure 3. Diagram outlining the process of photocatalysis on a TiO_2 film.

Figure 3 outlines how this effect makes TiO_2 useful as a self-cleaning material with current research looking into making the material more active on irradiation with visible light wavelengths. The composition of TiO_2 is a key factor in determining the photocatalytic activity of the film, i.e. what crystal forms are present. The different crystalline forms of titanium have different levels of photocatalytic activity. Anatase has the greatest activity so photocatalytic products aim to produce a higher proportion of this form and rutile TiO_2 has lower activity, brookite is the least active. The method of producing photocatalytic products should also be taken into account since other factors such as surface area and morphology are important for producing the best activity. For example, a fine granular structure provides a larger surface area for when electrons and holes can combine with water and oxygen to produce the radicals responsible for photocatalytic activity. Pure TiO_2 activates under UV light due to its band gap of 3.2 eV meaning only UV light has the correct energy to initiate photocatalysis[23].

There are different methods of testing the photocatalytic effects of TiO_2. Since photocatalysis is used to break down organic molecules methods can be used to detect particular molecules and analyse any change in concentration over time and possibly detect any new molecules being produced through breakdown. Detection can be done by methods such as gas chromatography and mass spectrometry. In order to gain insight into the rate of photocatalysis itself, observing the degradation of a coloured molecule such a methylene blue and measuring its change in absorbance over time can provide a faster and cost effective method[24-25]. An alternative is to use a fluorescent organic molecule that will lose its fluorescent as it degrades. The benefit of such methods is that the instrument will be more sensitive to a fluorescent signal at lower concentration levels. For the most efficient method of exposure to TiO_2, powders are often used that can provide an 80% breakdown within 1 hour of TiO_2 (anatase) and UV exposure[25]. This project however, required the TiO_2 to remain stationary opposed to freely mixing with the organic molecule. The solution was to utilise methods of TiO_2 film synthesis, otherwise removal of TiO_2 would be required as additional purification or sacrificing a substantial loss of material. This would lead to a relatively low rate of decay to be expected.

1.3.2 Surface Plasmon Resonance

Surface plasmon resonance (SPR) is a phenomenon that occurs on the molecular surface of precious metals such as gold and silver[26]. Plasmon refers to the oscillation of electrons or "plasma" on the metal surface. The coupling of light with surface plasmons causes enhanced fluorescent effects of certain range of light depending on the metal used. The oscillating plasmons provide additional electrons for fluorescence to occur, boosting the effect of any fluorescent already occurring (Figure 4).

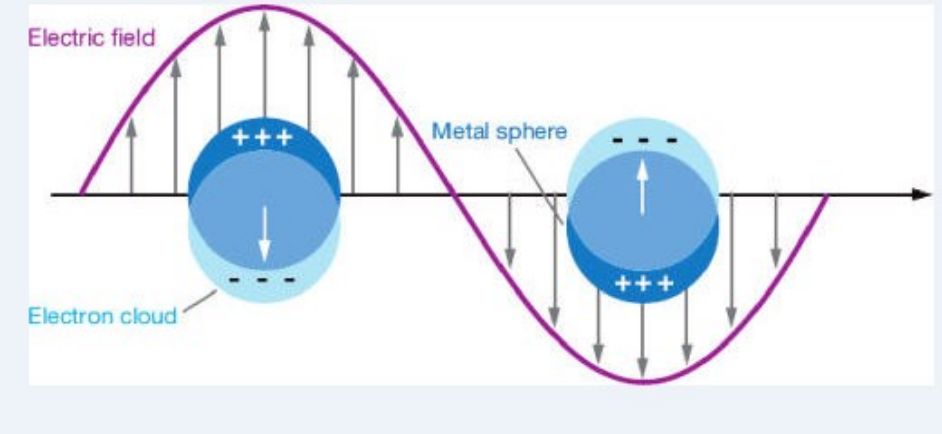

Figure 4. Diagram outlining the process of surface plasmon resonance on the surface of a metal nanoparticle when light is introduced [27].

An example of this is shown by coating a quartz substrate with a thin layer of noble metal[28], the author began with gold 50 nm in thickness, thin enough for the gold to exhibit surface plasmon resonance properties. A dye doped polymer layer was added 200 nm thick alongside a control sample covered with only the dye-doped polymer. UV light irradiated the samples and the emission of the coumarin laser dye (460 nm wavelength) was measured. The gold enhanced the emission two fold. The experiment however, was repeated by using a silver layer in place of gold and the emission was enhanced eleven fold. Figure 5 shows that the plasmon reflection can enhance or boost fluorescent dye emission but that it is also metal dependent, with certain metals being more effective at certain wavelengths than others. The report shows how SPR will enhance the

fluorescence properties of this project's nanomaterial system through boosting the fluorescence effect of fluorescent molecules.

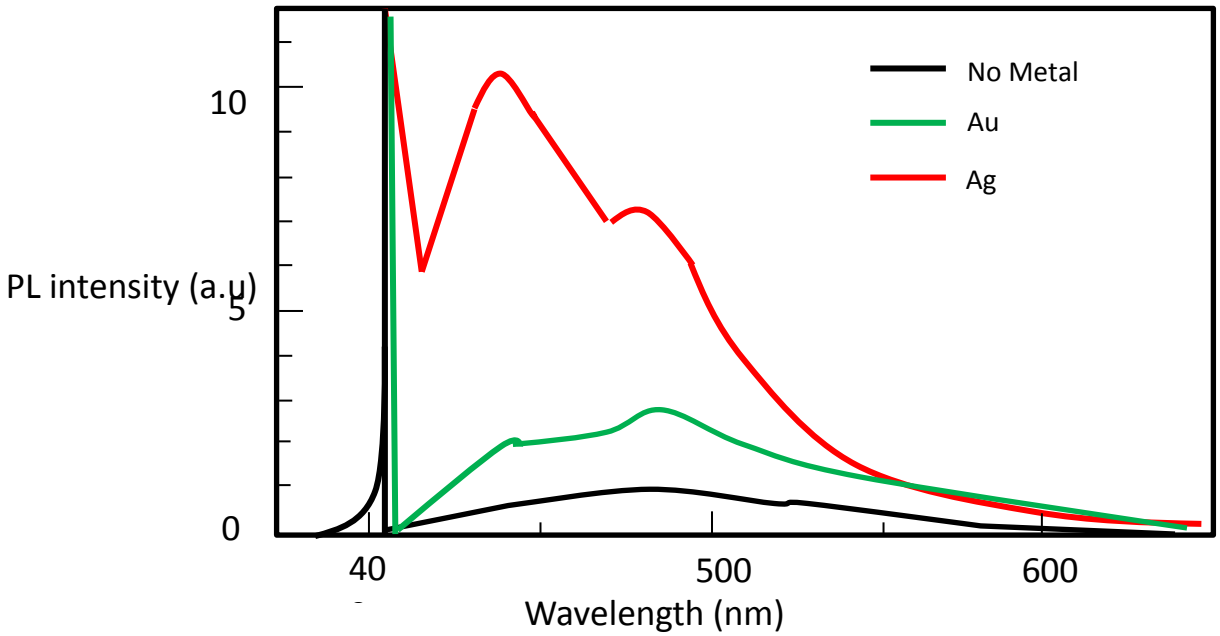

Figure 5. Photoluminescent spectra showing fluorescent enhancement due to gold and silver plasmon resonance [28].

This project investigated the way gold plasmon boosting can be used to affect photocatalysis of TiO_2. Rather than using a thin layer of gold as the previous study used, this project used gold nanoparticles. Gold nanoparticles are spheres ranging from 2-15 nm in diameter and possess the same plasmon affects as the 50 nm film, but with the added advantage of a greater surface area.

1.3.2 Magnetron Sputtering

Magnetron sputtering was the method used to produce the TiO_2 film indicated in this project. Other methods exist capable of fabricating a film, in particular the sol-gel method is popular involving a sol of TiO_2 to be prepared which is then dipped or spun onto a substrate, often quartz[29]. This sol is dried and then further sintering (heating) to form the crystals and provide the necessary film properties.

Magnetron sputtering however is a much more precise and repeatable method of coating thin films onto a substrate[30]. The process takes place in an evacuated sputtering chamber where the composition of the atmosphere can be carefully controlled. A high powered magnet or magnetron directs plasma of argon onto a specific target. The argon atoms bombard the target causing the surface atoms of the target to eject and deposit them onto the substrate surface (Figure 6). To produce TiO_2 films by this method a titanium target is used alongside a mixture of argon and oxygen gas. Once the titanium atoms are ejected from the target they easily react with oxygen and deposit onto the substrate as TiO_2.

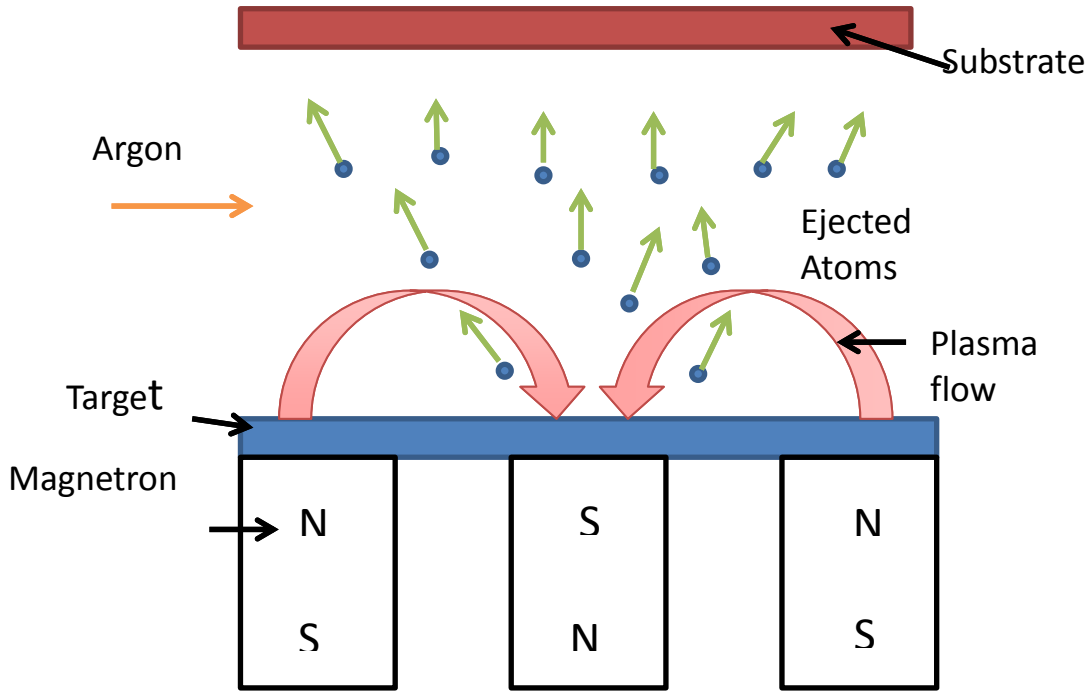

Figure 6. Schematic representation of the process that occurs during magnetron sputtering.

1.3.3 Fluorescent Molecules

Organic dye molecules were used as a model organic molecule as they show fluorescence, which provides an easy method of detecting via their photobleaching due to changes in molecular structure or chemical breakdown into colourless constituents.

A fluorescent molecule or chromophore possesses electrons capable of being excited to a higher energy level when interacting with certain wavelengths of light. When this electron returns to the ground state it emits a photon of energy depending on the distance between energy levels from which it came from. This light however is of a longer wavelength due to a loss of energy within the molecule called internal conversion shown in Figure 7. This ability to react to certain wavelengths of light means the organic molecules can be easily detected by their fluorescent signal and any loss in signal can be assumed to be due to change in molecule structure due to photocatalysis.

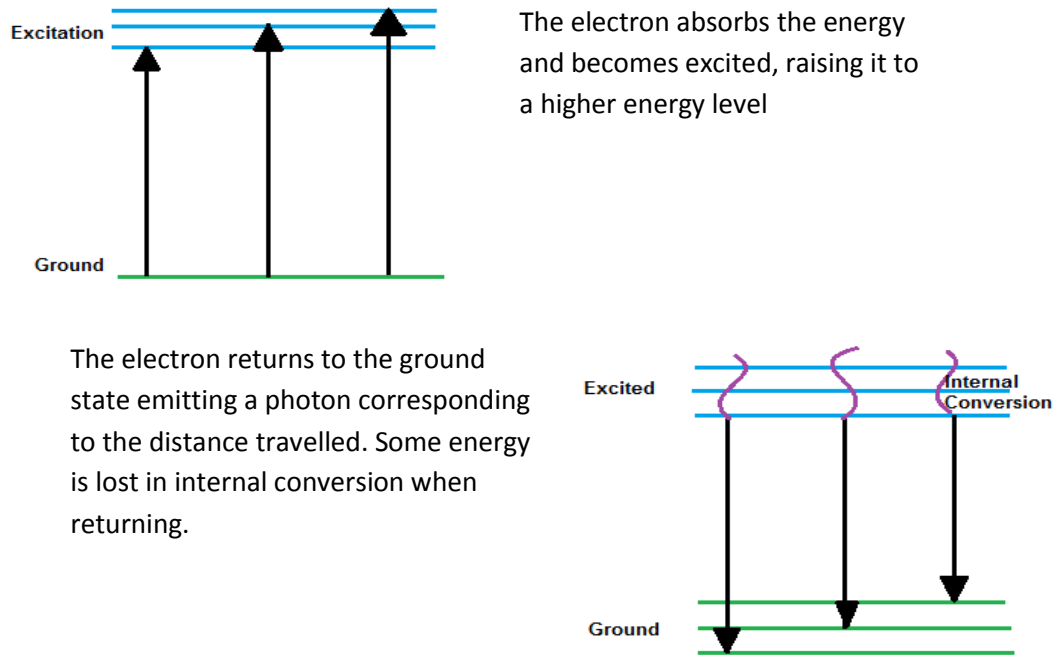

Figure 7. Schematic representation showing the movement of electrons between energy level that occur during the relaxation in the fluorescence process.

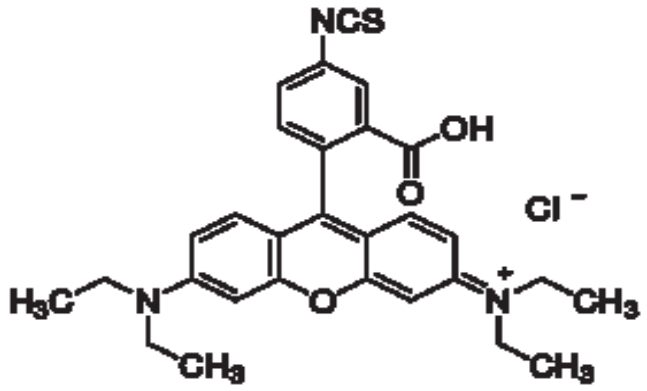

Figure 8. Molecular structure of Rhodamine B isothiocynate.

Rhodamine B isothiocyanate (RhB) (Figure 8) was used as the fluorescent dye in this project. The structure of RhB is very important in that the benzene ring structures provide the electrons capable of excitement and producing fluorescence. Changes to these structures leads to loss of this property known as photobleaching. This may not be a result of molecule breakdown into smaller molecules but just minor changes to the structure[31].

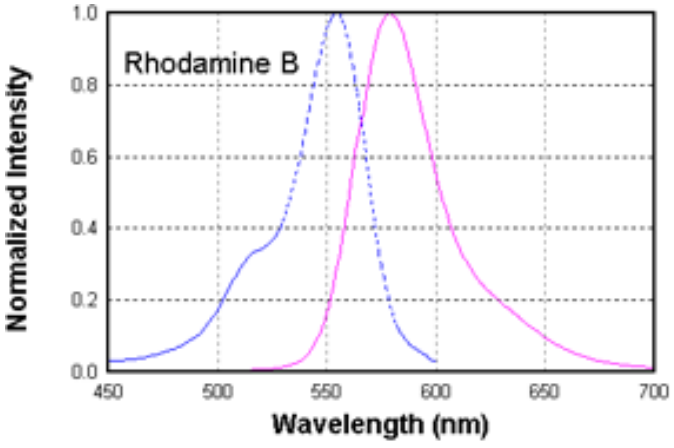

Figure 9. Fluorescence Spectrum of Rhodamine B dye showing excitation at 550nm (left curve) and emission at 580 nm (right curve) spectra.

The fluorescence spectrum of rhodamine B is shown in Figure 9. The left curve shows absorption with a peak centred at 560 nm, which is the excitation wavelength of the fluorescent dye. The right curve shows emission peak centred at 580 nm. The emission spectra wavelength increases from 560 nm to 580 nm indicating a loss of energy during the fluorescence process.

1.4 Nanoparticle Technology

Nanotechnology is an intense area of study possessing great potential in many areas of science with a huge variety of potential commercial applications[32]. Nanoparticles are usually defined as a particle less than 100 nm in diameter or less than 100 nm in any one of its other dimensions however many particles of a similar size are still referred to as nanoparticles for displaying unique properties that differ from the bulk equivalent. Properties such as fluorescence, super magnetism, surface plasmon resonance and other optical properties arise only at the nanoscale, largely attributed to a dramatic increase in surface area to volume ratio. These new properties provide the basis for new technologies to arise such as drug release studies in which a drug can be administered within a porous nanoparticle and released over time opposed to constantly varying the concentrations in the patient. They also allow the drug to be released in certain areas of the body preventing peripheral side effects and damage, for example localising a drug around the blood brain barrier[33].
In this project nanotechnology will be used to utilise the SPR effects of gold nanoparticles but also using other nanoparticles to help stabilize and potentially localise the gold to maximise TiO_2 photocatalysis.

1.3.5 Dye Molecule Capture Using Silica Nanoparticles

This project investigates the use of a TiO_2 film capable of breaking down organic molecules through UV light irradiation and their potential enhancement by SPR boosting from gold nanoparticles.

Silica nanoparticles where first fabricated by Stöber in 1968[34]. He used a method of polymerisation to combine a silica monomer (TEOS) while suspended in a solvent (ethanol) catalysed by ammonia. The following reaction occurs:

$Si(OC_2H_5)_4 + 2H_2O \longrightarrow SiO_2 + 4\ C_2H_5OH$ (in the presence of NH_3OH)

The initial silica produced nucleates and attracts other silica molecules to join it. After the first 10 minutes of the reaction no other nuclei form and instead build up to form larger and larger particles. This method of silica nanoparticle production forms the basis of the nanoparticle production methods used in this project.

In this project dye molecules must be encapsulated into the silica nanoparticle matrix. A modified dye molecule is used to enable this by adding an isothiocyanate group on the end, i.e. producing rhodamine B isothiocyanate. This group has no effect on the fluorescent properties of the molecule however it allows the molecule to form a conjugate with (3-aminopropyl)trimethoxysilane (APS) (Figure 10).

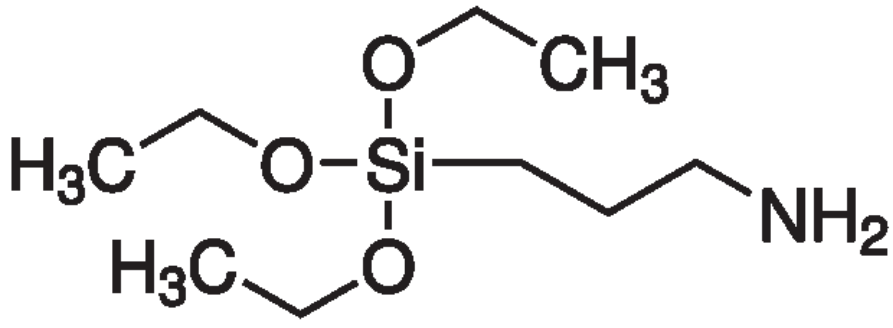

Figure 10. Molecular diagram of 3-aminopropyl trimethoxysilane.

The APS molecule once tagged with RhB is then able to polymerise with TEOS in the Stöber reaction utilising the Si-O-H_3C bonds and encapsulating the dye within the nanoparticle. The dye molecule will no longer be able to exhibit any chemical effects on the surface, however, it does not affect the fluorescent properties.

The initial concept is to produce a gold nanoparticle of 10-15 nm in diameter and coat this with a dye-silica shell (Figure 11). The gold core is capable of boosting the fluorescent signal of the dye while the silica matrix ensures the dye molecules are static and protected from any photobleaching.

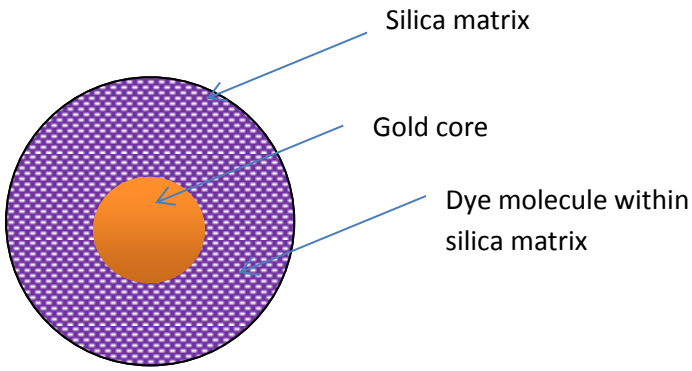

Figure 11. Schematical diagram representing the initial nanoparticle design.

The coating method used is based on a paper by Liz Marzan[35] and modified by Graf[36] however using an incorporated dye was originally proposed by Vrij [34].

1.3.6 Gold Nanoparticles

Gold nanoparticles provide the SPR properties necessary in this project. Gold colloids were originally synthesised and characterized by Turkevich[37]. The method involved reducing gold chloride with sodium citrate to generate gold atoms in suspension that would ultimately undergo nucleation and eventually nanoparticle formation.

$$2HAuCl_4 .4H_2O + 4Na_3C_6H_5O_7 \longrightarrow H_2 + 2Au + 4CO_2 + 4NaC_5H_5O_5 + 8NaCl + 8H_2O$$

The reaction is relatively fast taking only 20 minutes and this reflects on the size of nanoparticles produced being 10-15 nm opposed to silica that is usually 100 nm and can take over an hour to produce. Sodium citrate is not the only reducing agent capable of forming gold. THPC or tetrakis (hydroxymethy) phosphoniumchloride was also used in this project to produce even smaller gold nanoparticles (1-3 nm). THPC is a much faster acting reducing agent and hence why the particles are much smaller [38]. Additional gold can be added by using another reducing agent when in the presence of gold salt ($HAuCl_4 + K_2CO_3$). Hydroxylamine hydrochloride was used in the project to attempt to create a gold shell around a silica-dye nanoparticle and investigate the change in fluorescent properties[39].

1.3.7 Zeta Potential

Zeta potential is an important concept in nanoparticle technology. It is the electric potential between the particle surface and the medium in which it is suspended. This potential difference allows the medium to provide a "slippery layer" to prevent surfaces from interacting and possibly aggregating [40] (Figure 12).

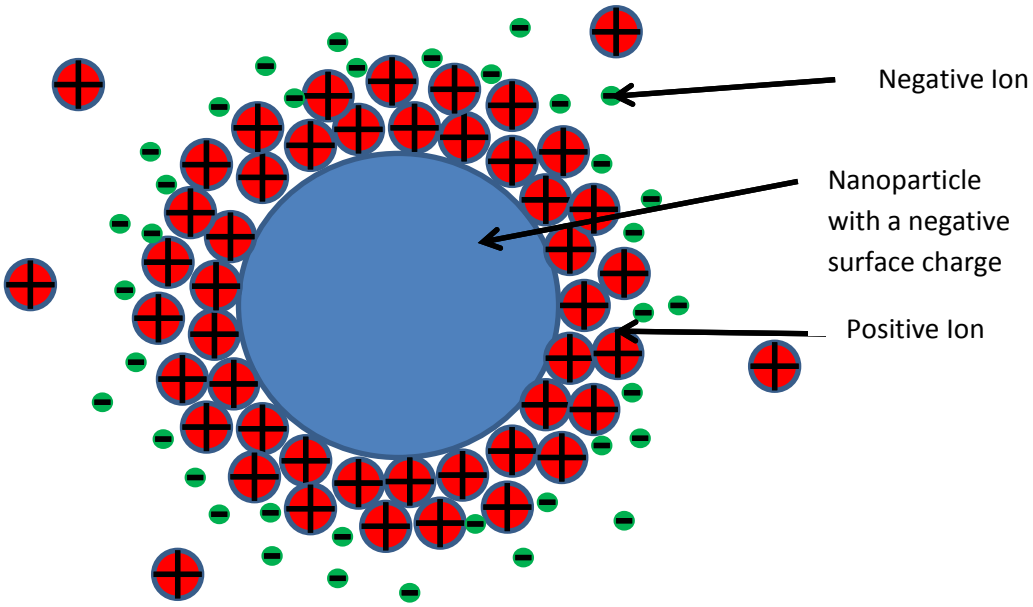

Figure 12. Diagram showing the effect of the media is creating a stable particle from its zeta potential.

In the case of gold nanoparticles for example citrate ions are used to prevent the positively charged gold from aggregating with other particles. These citrate ions are coincidently produced during their synthesis[37]. When in ethanol, there are no ions to provide this and so the suspension turns from ruby red corresponding to nanoparticles of 15 nm to black indicating aggregated particles. To prevent this without changing the medium, steric bonds can be added to the gold surface which physically separates the nanoparticles by using a polymer to prevent them from touching (Figure 13). This project uses this property by functionalising the surface with polyvinypyrrolidone of molar mass 10,000 (PVP) when coating gold colloids with silica in an ethanol medium. Placing gold colloids

in ethanol would normally cause them to become unstable and coagulate. Adding steric bonds can however affect the surface properties over time making it unable to take part in further modification leaving the sample useless and eventually losing the ability to maintain stability.

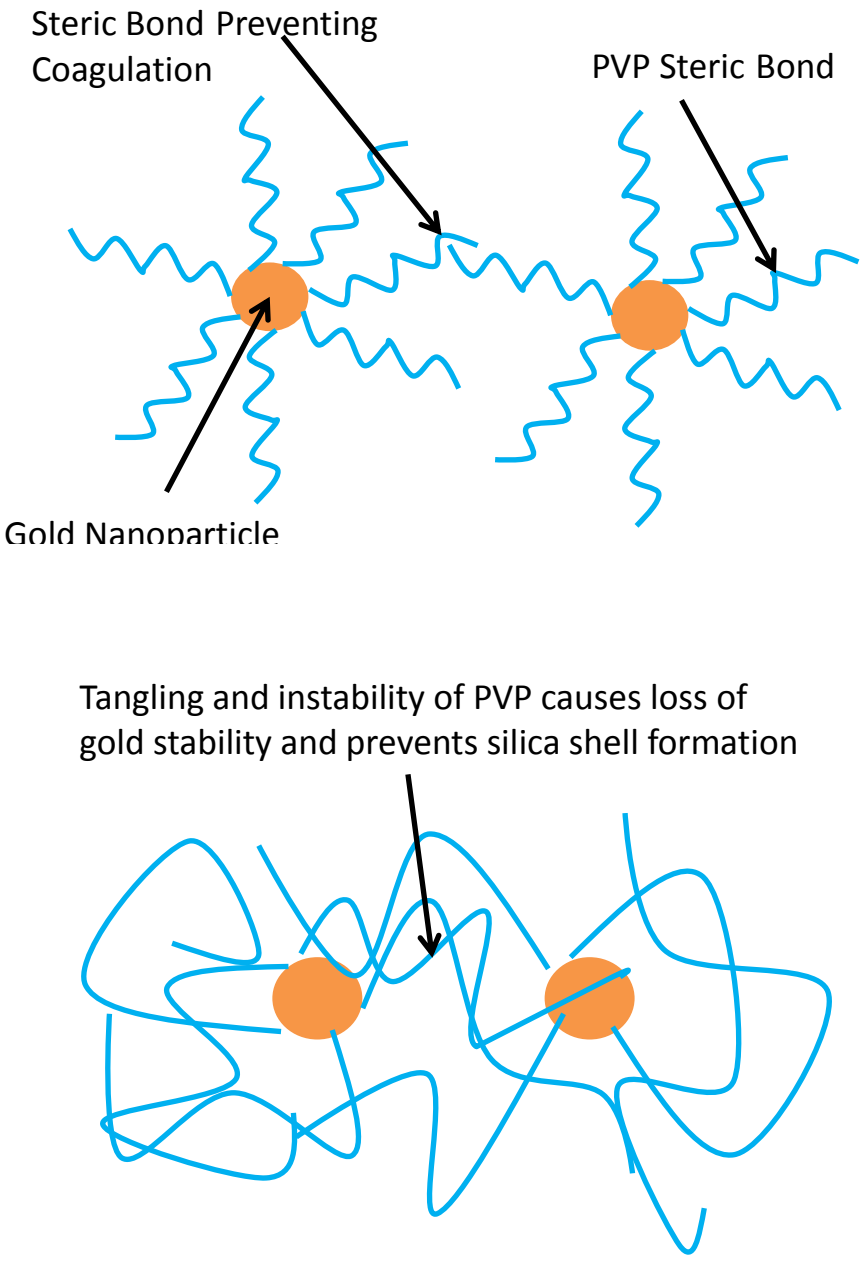

Figure 13 Diagram outlining the effect of steric bonds and their short effective lifetime

2. Experimental

2.1 Fabrication of Nanoparticles

Four distinct types of nanoparticle were synthesised for photocatalytic testing with TiO_2 to investigate their unique properties outlined in Figure 14.

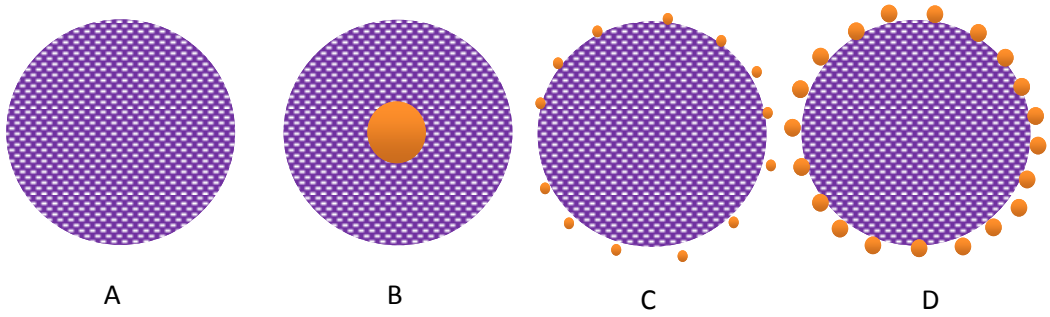

Figure 14. Various nanoparticles synthesised to test the effect of gold plasmon boosting of TiO_2 photocatalysis. A is a silica-dye nanoparticle, B a gold core silica-dye shell, C Silica-dye nanoparticle coated in gold seeds, D silica-dye nanoparticle coated in a gold nanoshell.

This section will describe the different methods used to synthesise these nanoparticles, how they were characterised and the experiments of photocatalysis with TiO_2.

Table 2. List of the chemicals and materials used in the following experimental

Chemical Name and Purity	**Source**	**CAS Number**
3-(Aminopropyl)triethoxysilane (99 %)	Sigma Aldrich	919-30-2
Ammonia Solution (29 % wt)	Sigma Aldrich	7664-41-7
Gold Chloride (99 %)	Sigma Aldrich	27988-77-8
Ethanol (4.8 % denatured methanol)	Fletcher Chemicals	64-17-5
Fluorescein (≥90 %)	Sigma Aldrich	2321-07-5
Polyvinylpyrrolidone (mol wt 10,000) (100 %)	Sigma Aldrich	9003-39-8
Rhodamine B isothiocyanate (95%)	Sigma Aldrich	36877-69-7
Sodium Citrate (anhydrous) (≥99 %)	Sigma Aldrich	6132-04-3
Sodium Hydroxide (anhydrous pellets) (≥99 %)	Sigma Aldrich	1310-73-2
Tetraethyl Orthosilicate (99.9 %)	Sigma Aldrich	78-10-4
tetrakis(hydroxymethy)phosphonium chloride (THPC) (80 % in H_2O)	Sigma Aldrich	124-64-1
Potassium Carbonate (≥99 %)	Sigma Aldrich	584-08-7

2.1.1 Synthesis of Silica Particles

Synthesis of silica nanoparticles used the established method by Stöber [18] by using a silica monomer such as TEOS and polymerizing using ammonium hydroxide as a catalyst and reactant (the H_2O) in ethanol medium.

Ethanol (90 ml) was poured into a 250 ml round bottomed flask. A separate dilution of TEOS (0.25 ml) was added to ethanol (10 ml) in a 50 ml beaker and gently stirred. The TEOS mixture was added to the ethanol and mixed for 1 minute under magnetic stirring at 300 rpm. Ammonium hydroxide (29% wt) (3.5 ml) was introduced during stirring and left to react for 5 hours at 25^{o}C (Figure 15). When the reaction was completed the product was centrifuged at 15,000 rpm for 20 minutes. The supernatant was removed with a pasteur pipette and the remaining suspension was re-dispersed in ethanol (90 ml). The procedure was repeated to ensure residual reactants are no longer in the silica nanoparticle suspension.

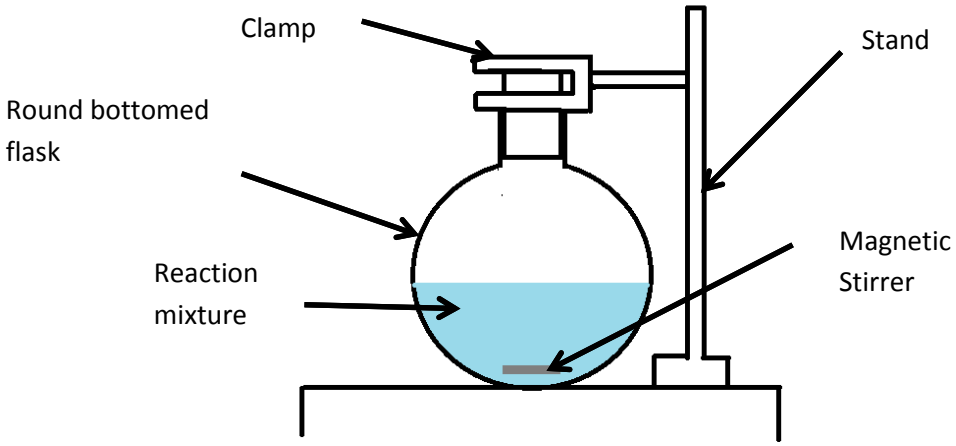

Figure 15. Schematic representation of the apparatus set up used in fabricating silica nanoparticles.

2.1.2 Synthesis of Silica-Dye Nanoparticles (Particle A)

Incorporation of dye to silica in a monodisperse nanoparticle was first demonstrated by Van Blaaderen et al [36]. The preparation coupled the dye (rhodamine B isothiocyanate) with a silane coupling agent (APS) and incorporating this into the Stöber reaction or alongside a different catalyst such as Sodium Hydroxide (NaOH).

To Prepare the dye, APS conjugate rhodamine B isothiocyanate (0.001 g) was dissolved in ethanol (1ml), then APS (0.1 ml) was added and allowed to react for 12 hours in dark conditions (covered in foil) under magnetic stirring at 300 rpm. The conjugate was stored in dark conditions.

TEOS (0.15 ml) is used along with the full amount of APS + dye in ethanol (1.1 ml). These were added to ethanol (90 ml) in a round bottomed flask under magnetic stirring at 300 rpm. NH_3OH (29 % wt.) (3.5 ml) was introduced to initiate the reaction. The reaction took 5 hours at 25^{o}C. After 5 hours the product was purified by centrifuging at 12,000 rpm for 20 minutes, removing the supernatant and resuspending in ethanol. Centrifuging was performed twice to ensure all reactants were removed.

Alterations to the above procedure were performed with the aim of producing particles of different morphology. Alterations were made to the amounts of materials used and the timing of the reaction however all other apparatus and conditions remained the same. The following table outlines the different conditions used.

Table 3. Conditions used in producing silica-dye nanoparticles.

Reaction Attempt	**TEOS(ml)**	**APS(ml)**	**RhB(ml)**	**NH_3OH(ml)**	**Ethanol (ml)**	**Reaction Time (h)**
1	0.15	0.01	0.001	3.5	90	5
2	2.83	0.067	0.010	5.1	57	5
3	3.54	0.067	0.010	4.3	100	3
4	1.5	0.1	0.001	2	30	12
5	1.5	0.1	0.001	3	50	2
6	1	0.1	0.001	3	40	2h 20

2.1.3 Gold Nanoparticles

Synthesis of gold nanoparticles uses the method based by Turkevich et al [37]. Gold chloride tetrahydrate (0.011g) was measured out using a glass pipette and dissolved in distilled water (10 ml) in a 50 ml beaker. This solution was added to near boiling distilled water (80ml between 80-90^{o}C) in a round bottomed flask under 300 rpm stirring. The mixture was taken off the heat to slowly cool. Sodium citrate was prepared as a 1% solution (0.1 g in 10 ml) in a 50 ml beaker and sonicated to ensure it is completely dissolved. The solution was then added to the reaction mixture (3.5 ml of prepared solution). The reaction remained under stirring for 30 minutes. After 5 minutes the mixture turned from a pale yellow/clear to a dark blue. The mixture would gradually go from blue to a deep purple and eventually a wine red like colour after 20 minutes (Figure 16). Once the colour of the mixture had completely changed (after 30 min reaction time) the gold nanoparticle suspension was ready and stored at room temperature, in the dark.

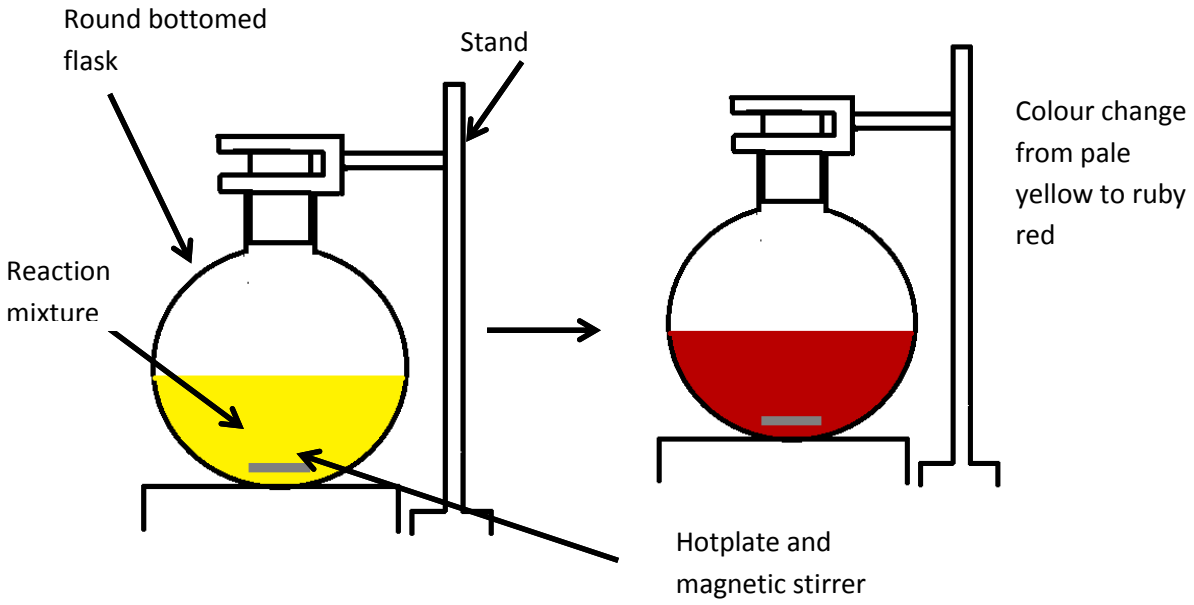

Figure 16. Schematic representation of the apparatus set up used in gold nanoparticle fabrication, including the colour change.

2.1.4 Synthesis of gold core silica shell nanoparticles

Gold nanoparticles were first PVP functionalised before the shell growth process. PVP (1.25 g) was dissolved in distilled water (50 ml) requiring vortex mixing and sonication to ensure all the powder had dissolved. PVP solution (3.5 ml) was added to gold suspension as prepared (50 ml) in a 100 ml beaker. The mixture was left under magnetic stirring at 300 rpm for 15 minutes. The mixture was centrifuged after this time at 8,000 rpm for 10 minutes to remove any remaining PVP and resuspended in ethanol (50 ml). This mixture would have to be used within 1 week of preparation. This PVP functionalised suspension was used in the following coating process.

TEOS solution (0.25 ml in 10 ml ethanol) was prepared in a 50 ml beaker. PVP functionalized gold particle suspension (5 ml) was added to ethanol (80ml) in a round bottomed flask. Ammonia hydroxide (29 % ammonia in distilled water, 3.5 ml) was then added under stirring at 300 rpm. TEOS solution (2 ml) was then added to the mixture. After 1 hour additional TEOS was added (2 ml) and again every hour, continuing for 4 hours. After a final hour of reacting the mixture was centrifuged at 15,000 rpm for 20 minutes and resuspended in ethanol.

The product was characterized using PCS to determine particle size, TEM to analyse structure since this method will allow imaging of the gold core with a shell. Particles will also be of sufficient size to be visible under SEM to provide more evidence of size and dispersion. UV-vis was useful to determine the amount of gold and silica present in the product.

An additional method for producing gold core silica shell nanoparticles was investigated using sodium hydroxide (NaOH) [42]. A TEOS solution was prepared (0.25 ml in 10 ml ethanol) separately while PVP functionalised gold nanoparticles (5 ml), distilled water (24 ml) and NaOH (4 ml of 10M solution) was added to ethanol (66 ml). TEOS was added drop wise using a Pastur pipette at a rate of approximately 1 drop per second at room temperature. The reaction was left for 12 hours and centrifuged at 10,000 rpm for 20 minutes, resuspending in ethanol.

2.1.5 Synthesis of gold core silica+dye shell nanoparticles (Particle B)

Rhodamine B isothiocyanate (0.001 g) was measured out into a glass bijou (10 ml) along with a flea stirrer using a disposable plastic measuring spatula, this equates to 3.22 $x10^{23}$ molecules in each reaction. Nitrogen gas is gently introduced via a tube to remove oxygen from the bijou however a high flow was not used to avoid liquid and powder to blow out of the bijou and quickly sealed after 1 minute of blowing. APS (0.01 ml) is measured out using a pipette and added to the rhodamine B isothiocyanate along under a constant stream of nitrogen. Nitrogen was also bubbled into the APS bottle before storage. Stirring at 300 rpm and maintained in dark conditions for a minimum of 2 hours. The mixture should turn an amber colour.

Once the dye and APS complex was complete it takes part in the normal silica coating reaction. Instead of adding a 2nd injection of TEOS solution, add the dye-APS conjugate. Continue adding the TEOS solution as normal, however, leave out the final injection.

A method was also investigated using NaOH as the catalyst as an adaptation by Kobayashi et al[42]. TEOS (0.02 ml) was diluted in ethanol (10 ml) in a separate 50 ml beaker. Ethanol (35 ml) was added to a 200 ml round bottomed flask along with the TEOS solution, NaOH (6 ml of 1.5 $x10^{-3}$ M solution), distilled water (11 ml), gold nanoparticle suspension (0.85 ml) and APS-dye conjugate (9.2 x 10^{-5} ml). React for 5 hours and centrifuge at 15,000 rpm for 20 minutes. Resuspend in ethanol.

Table 4. Summary of the different conditions and concentrations used for the NaOH method

Gold Nanoparticles	**TEOS**	**NaOH (ml of 1x10^{-4} M)**	**H_2O (ml)**	**APS-Dye (ml)**	**Ethanol (ml)**	**Time (hr.)**
0.0847	1.94 x 10^{-2}	6.5	12.77	9.2 x 10^{-5}	70.74	5
0.847	9.71 x 10^{-4}	1.58	17.68	9.2 x 10^{-1}	70.74	5

The previous stated characterisation techniques should be used (i.e. SEM, TEM, UV-VIS, PCS). However, as the new particles have fluorescent properties, the fluorescence can be measured. The fluorescence spectrophotometer was set to a range of 500-700 nm using the excitation of

rhodamine B at 550 nm and emission at 580 nm. The sample of suspension was diluted before measuring by taking 1 ml of suspension and adding this to ethanol (9 ml). This sample was then added to a quartz cuvette and placed in the fluorescence spectrometer for analysis.

To provide evidence of plasmon boosting, coreless silica and dye nanoparticles were synthesised as references. This was the same method of coating, however, the initial mixture had no gold nanoparticles. Therefore the silica would nucleate new particles and grow from these, containing the same amount of dye.

2.1.6 Synthesis of Silica-Dye Core Nanoparticles Coated in Gold Seeds (Particle C)

The method to produce the silica-dye nanoparticle remained the same however gold seeds were attached to the surface of the nanoparticle to produce an alternative method of producing plasmon boosting.

Gold seeds are produced by reducing gold chloride with THPC. The nanoparticles produced using this method will be much smaller than using sodium citrate, 1-3 nm in diameter opposed to 10-15 nm.[38] NaOH (0.5 ml of 1 M) was prepared in distilled water (45 ml) with THPC (12 µl in 1 ml H_2O) and stirred for 5 minutes. After this time $HAuCl4.3H_2O$ (2 ml of 1% solution) was added quickly to the mixture which turned from yellow to a rust brown colour. This gold seed suspension was later used in the attachment process.

An aliquot of silica nanoparticles (50 ml) was heated to 80^{o}C and APS (0.01 ml) was added remaining under magnetic stirring for 1 hour at 300 rpm. After this time the mixture was centrifuged at 6000 rpm for 10 minutes and resuspend in ethanol.

To attach gold seeds to APS functionalized silica nanoparticles, gold seed suspension (2 ml) was added to the APS functionalised silica-dye nanoparticle suspension (50 ml). This was mixed vigorously for 30 seconds then left static for 2 hours at room temperature. Centrifuged at 6000 rpm twice to ensure all unattached gold seeds are removed and resuspend in ethanol.

2.1.7 Silica Core Nanoparticles With a Gold Nanoshell (Particle D)

Growth of the nanoshell required a mixture of potassium carbonate (0.025 g) and gold chloride (1.5 ml of 1 % solution) in distilled water. The solution would appear yellow at first but turn clear after 30 minutes. The gold salt formed can be left covered in the dark for 24 hours to produce “aged gold”. The silica gold seed suspension (0.2 ml) was then added to the gold salt mixture (4 ml), under

vigorous magnetic stirring. Hydroxylamine hydrochloride solution (1.87×10^{-3} M) was prepared and added drop-wise to the gold salt and nanoparticle mixture until a colour change to blue was visible. This colour change indicated that the gold seeds on the particle surface had grown and eventually joined together to form the Nanoshell. Additional hydroxylamine hydrochloride would increase the ultimate thickness of the shell, as more seeds to combine resulting in a thicker shell. In this project 10 ml of hydroxylamine hydrochloride solution was added. Centrifuged at 4000 rpm for 10 minutes and the particles resuspended in ethanol.

2.2 TiO_2 Film Growth

In order to grow TiO_2 films a rectangular stainless steel vacuum chamber was used with internal dimensions of 1800 mm long, 650 mm wide and 300 mm high. The vacuum chamber was used as a large area coating chamber manufactured by Prevac Sp.2.0.0. The chamber has the capacity for 2 rectangular magnetrons side by side. The chamber would be pumped down by diffusion pump backed by a rotary pump with a typical base pressure of 2-3 x 10^{-5} Pa measured by a Penrings gauge (manufactured by Edwards Ltd.

The substrate used for magnetron sputtering was a clear glass microscope slide. The slide was cleaned with isopropanol and dust removed by blowing air on the surface. A line of marker pen was drawn on the middle of the surface to be sputtered to later aid in measuring the thickness of the film. The glass substrate was placed on an aluminium substrate stand 90mm from the target within the sputtering chamber, which was closed ensuring the chamber was sealed.

The magnetron was fitted with a solid titanium target 100 mm wide and 300mm long with the chamber evacuated to a pressure of 3.2 x 10^{-5} mbar. This was achieved by roughing the chamber with a rotary pump initially then with the addition of a diffusion pump the pressure can continue to decrease. Once the chamber reached the required vacuum pressure, water cooling was introduced to prevent the target from burning out. Argon gas was added at a flow of 31 sccm by an MKS mass flow controller (MKS PR 4000). The power source was then turned on with varying settings. Settings where initially 1000 W of power, 300 volts, 3 Amps of current, frequency of 100 kHz, off time 5µs and an operating pressure of 3.6 mTor. Before the film was grown the target had to be cleaned by having the power onto the target while a screen was used to prevent any sputtering onto the substrate. This cleaning was performed for 10-15 minutes, however it could be observed since the plasma colour changed from flashing pink to an even violet. Rotation was used on the target to produce a more even film. Sputtering was performed for one hour, initiated by removing the dividing screen. To stop sputtering the power supply was first turned off, then rotation, then the gas

supply and then the water cooling pump. The substrate was left to cool for an equivalent time that the sputtering has been performed for, i.e. 1hour 15 minutes. During the production of different films these settings were slightly altered to produce variable results, notably film quality and thickness.

Table 5 Different settings for production of TiO_2 films by magnetron sputtering.

Sample name	**Off Time µs**	**Frequency (kHz)**	**Voltage (V)**	**Current**	**Reaction time (min)**
TiO_2 20/01/12	5	100	500	2.5	60
TiO_2 24/01/12	5	100	300	2.5	60
TiO_2 25/01/12	5	100	300	3	108
TiO_2 26/01/12	4	100	400	2.6	120
TiO_2 30/01/12	5	100	450	2	120
TiO_2 03/02/12	4	20	500	2	120
TiO_2 08/02/12	5	100	450	2.2	120
TiO_2 10/02/12	5	100	400	3	120
TiO_2 15/02/12	4	100	350	2.2	120

To measure the film thickness, the line of ink produced using the marker pen (before sputtering) is removed using a tissue soaked in ethanol as shown in Figure 17. This created a step between the sputtered film and unsputtered glass that could be measured by Dektak Profilometry.

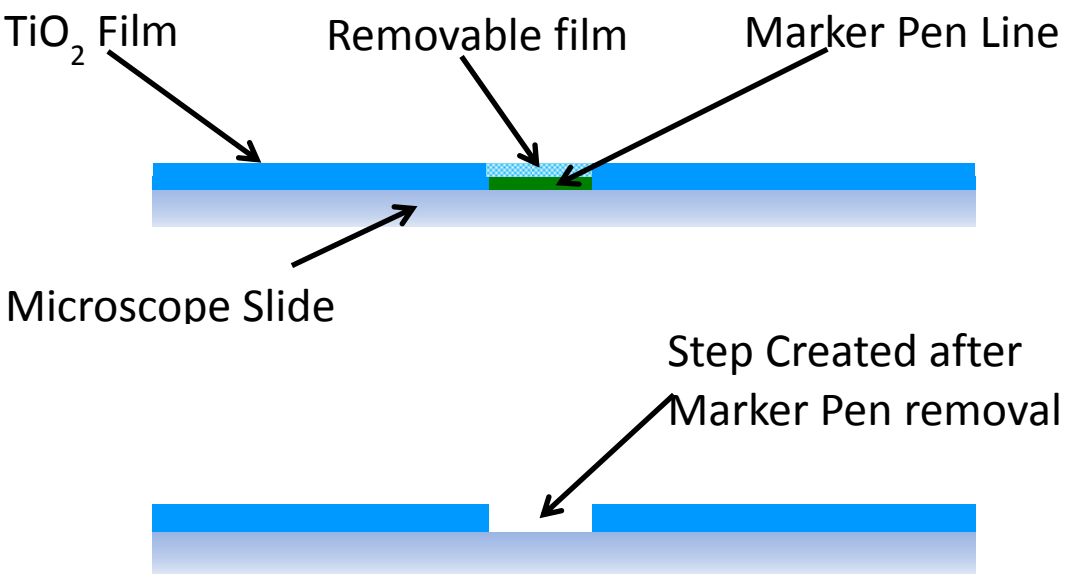

Figure 17. Schematic of creating a TiO_2 film step using a marker pen and removing with ethanol and tissue.

2.3 Characterisation

Different characterisation techniques were used to analyse the samples produced. Full analysis was necessary since nanoparticles in particular need to be sized, quantified, and their morphology analysed. Different techniques were then used to evaluate the functional parts of the products such as fluorescence and photocatalytic properties. Table 6 outlines the different types of sample made in this project and what different characterisation methods where used on them.

Table 6. Different characterisation techniques performed on different samples.

Sample type	**SEM**	**TEM**	**DLS**	**Spectrophotometer photometer**	**Fluorescence**	**Step nanotribology**
Gold NP	-	yes	Yes	yes	-	-
Gold Silica Shell NP	-	yes	Yes	-	-	-
Gold core Silica+Rh B NP	-	yes	Yes	-	yes	-
Silica-dye NP	-	yes	Yes	-	yes	-
Gold core Silica+Rh B NP (NaOH Method)	-	yes	yes	-	yes	-
Silica NP	-	yes	-	-	-	-
Silica core gold seed coating	Yes	Yes	-	Yes	Yes	-
RhB solution	-	-	-	-	yes	-
TiO_2 films	yes	-	-	yes	-	yes

2.3.1 Scanning Electron Microscopy (SEM)

JEOL JSM-5600LV scanning electron microscope was used for this project. The SEM was capable of viewing at up to x 50,000 magnification. For the TiO_2 films chips 1cm x 1cm squares were cut from the coated slide with a glass cutter and bonded to an aluminium stub. The aluminium stubs were then placed into their assigned spaces in the sample holder within the chamber. The chamber was evacuated to allow viewing of the sample. In order to achieve a quality image a low scan rate is required to enhance visible details. Images were taken at x5000, x20,000 and x50,000 magnification. This magnification was required in order to view the individual crystalline structures on the film surface.

To view nanoparticle samples a drop of suspension was added to an aluminium stub and allowed to dry. The stub was then coated in a thin layer of gold using an EMITECH SC7460 sputter coater. The chamber was evacuated to 4mbar. The anode voltage was set to 800 V and the argon bled in to produce an anode current of 10 mA. The sputtering process continued for 2 minutes, after which time the leak valve was closed, the chamber and vented. The coated sample is then imaged in the SEM using the same method as for the TiO_2 substrates.

2.3.2 Transmission Electron Microscopy (TEM)

For TEM imagery the nanoparticles were placed onto 300 mesh formvar coated copper film grids. To prepare a sample on the TEM grid, the sample suspension was first diluted to 1/10 of its initial concentration so that the particles would not appear overcrowded on the grids and provide a clear image. A drop of the sample was placed onto the grid whilst holding in a warm atmosphere or oven by tweezers. The grid was allowed to dry and the prepared sample was returned back into the allocated slot in the grid case. Once prepared the TEM grids are placed individually into the

microscope. The magnification used reached x200,000 in order to view nanoparticles 50 nm in diameter and smaller. Images were taken for both a distant/perspective view and high magnification images of individual nanoparticles.

2.3.3 Photon Correlation Spectroscopy (PCS)

For PCS the Malvern Zetasizer nano was used to measure the size of particles in a particular sample and produce a graph of particle number against particle size. The method also provides an average particle size and particle size distribution. Particle size was measured by taking a drop of sample suspension and placing into a polystyrene cuvette containing distilled water. The instrument was then programmed to size the particles in the sample depending on the substance, i.e. silica or gold. The instrument provides the graph of results of number of particles against particle diameter, while also providing information on the mean size and poly dispersity index (PCI). PCI is a measurement of how uniform the particle sizes are, with 1 being extremely polydispersed and <0.07 being uniform or monodisperse.

2.3.4 Zeta Potential

The Malvern Zetasizer Nano was also used to measure zeta potential. This was used on some samples as a method of determining the stability of a nanoparticle suspension. The method uses the same machine as PCS, i.e. the Malvern Zetasizer. The method, however, does not use clear cuvettes but diodes capable of measuring the potential difference of a sample. A few drops of the sample is added to the capillary cell using a pasture pipette and inserted into the machine. The medium used does not have to be considered so the sample can be immediately measured. The machine provides a value of the zeta potential in electron volts (eV).

2.3.5 UV/VIS Spectrophotometer

The Perkin Elmer Lambda 40 UV/VIS spectrometer was used to measure absorbance of light wavelengths in particular samples. This was used to quantify certain samples such as gold, specifically when calculating the amount of gold being used in each experiment and rhodamine dye

during the photocatalytic breakdown experiment. In order to gauge the gold concentration a calibration graph was created. A sample was taken of known gold concentration and measured, and the peak transmittance was taken. The sample was then halved in concentration and another peak was taken. This systematic dilution was continued and a graph was produced plotting gold concentration against absorbance. This could be used to determine the gold content of unknown samples, particularly after centrifugation purification.

2.3.6 Fluorescence

The Perkin Elmer LS 55 Luminescence spectrometer measured the light fluorescing from a sample when illuminated by certain wavelengths. It was important to set an adequate range for the instrument to test from so that both the excitation and emission could be observed. The only fluorescent molecule used for testing was Rhodamine B, with an excitation at 550 nm and emission at 580 nm so the Excitation wavelength was set to 550 nm with a peak expected at 580 nm. This required the measurement range to be set between 400 and 700 nm. Once the range was set 3 ml of the sample suspension was added to a quartz cuvette and the measurement performed, producing a graph usually including an excitation peak and emission peak. Quartz was required in order to not produce any unwanted emission peaks that a plastic cuvette will produce. These measurements were used as part of photocatalytic tests.

2.3.7 Dektak Profilometry

Dektak Profilometry (Dektak® 3 stylus profilometer manufactured by Vecco Instruments Inc) was used to measure the step indentation for a sputtered film. The glass substrates were prepared before sputtering to provide a step between the sputtered film and bare glass, as described in section 2.2. The films were mounted onto the step machine and microscope imagery allowed the step to be lined up with the measurement needle. The needle used does not touch the sample but relies on atomic forces to determine the distance between itself and the sample. The needle then moved across measuring the relative height of the film producing a two dimensional graph/image (Figure 18). The difference in height between the TiO_2 film and bare glass was then calculated. Several repeatable measurements along the step line were in order to produce an average value.

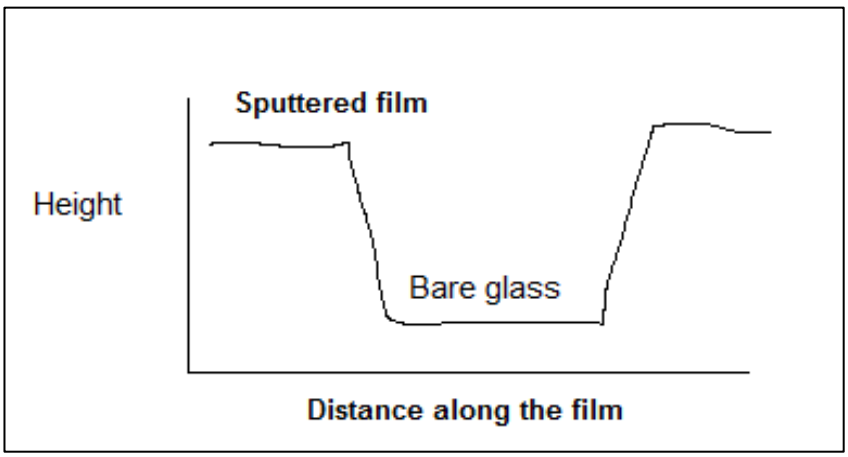

Figure 18. Schematic representation of a Dektak Profilometry two dimensional graph for measuring the thickness of a film.

2.3.8 Raman Spectroscopy

Raman spectroscopy (Renishaw in via spectrophotometer with a 514,4 nm argon laser) is a powerful technique in analysing the chemical structure and physical form of TiO_2 photocatalytic films[39]. This is achieved by shining the argon laser onto the sample causing the molecules electron cloud to become polarised, causing then to rise to a higher energy state. This creates a virtual state of the molecule which is unstable resulting in the energy being released from the molecule. The scattering of this ejected light creates a distortion field that can be measured. This scattering relates to the chemical structure of the samples molecules, providing information on their chemical composition, in particular what forms of TiO_2 are present and in what quantities, i.e. anatase, rutile or brookite. The samples were cleaned gently with ethanol before measurements and a central measurement of the sample was found with the aid of a light microscope.

2.4 Photocatalytic Testing

Photocatalytic testing measures the activity of TiO_2 and its ability to break down organic molecules. A solution of methylene blue of concentration to give an absorbance of 1 was first produced. To determine basic activity of TiO_2 a piece of TiO_2 film (2cm x 2cm) was cut out and placed into a 50 ml beaker filled with 10 ml of the methylene blue solution. The beaker was placed under the UV lamp (360 nm wavelength, 1147 $\mu W/cm^2$ intensity at 2") and used for the absorbance of the mixture measured every hour for 5 hours using UV/Vis spectroscopy. The rate of degradation can be determined from the shape of a peak absorbance versus irradiation time plot. This value was compared to a control without a catalytic film so that the UV photobleaching could be taken into account and the actual photocatalytic activity could be found. The effect of the TiO_2 film in combination with the various nanoparticles produced was then investigated using the same method as five different samples. The RhB molecule concentration was 3.22×10^{22} molecules/ml for catalysis

on all samples. This includes those that did not have RhB encased within the nanoparticles, the same concentration used during synthesis.

As RhB is a fluorescent dye, fluorescence spectroscopy was in preference to UV/Vis spectroscopy. The fluorescence spectrophotometer was therefore programmed for rhodamine B (λ excitation 550 nm and λ emission 580 nm).

An additional investigation was performed in order to determine the effect of gold seeds on TiO_2 photocatalysis. Using four (2cm x 2cm) square TiO_2 films placed in 50 ml beakers, two contained rhodamine B solution (50 ml 0.01 g/L distilled water)(1.61×10^{22} molecules), two contained the same rhodamine B solution (0.01 g/L distilled water) with 1 ml gold suspension (15 nm diameter, 1.546×10^{18} particles per ml). An additional beaker containing rhodamine B (50 ml 0.01 g/L in distilled water) without a TiO_2 film, was used as a control. These samples were also irradiated with UV light, however, as the gold would possibly alter the fluorescence results of the sample, UV/VIS spectroscopy was used to monitor the photo degradation of the dye.

3. Results and Discussion

The results for this project were derived from the various characterisation and analytical techniques used, described in section two.

3.1 Fabrication of Nanoparticles

3.1.1 Silica Nanoparticles

This section will present the results of silica nanoparticle fabrication

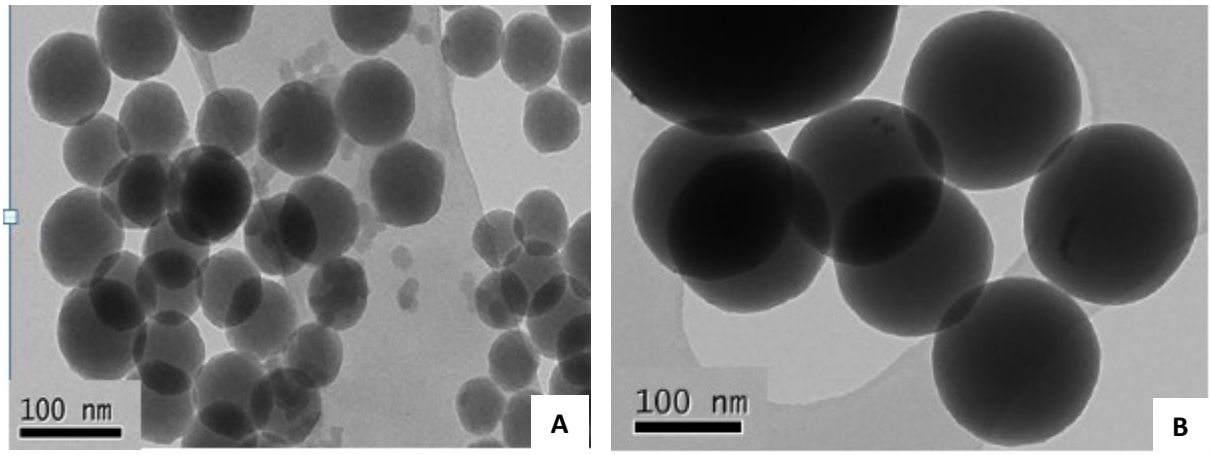

Figure 19. TEM images of silica nanoparticles prepared using the Stöber method.

Silica nanoparticles where fabricated as planned using the method by Graf et al[36]. Although not the primary type of nanoparticle required in this project, forming adequate silica nanoparticles first was needed to form a basis in terms of what methods to use in the future and what to avoid. Figure 19 shows TEM images of some silica nanoparticle samples produced. These samples where relatively uniform however there was a mixture present as seen in Figure 19 A where the majority are between 90-80 nm in diameter however some go larger than 100 nm and some are much smaller and not spherical at all. Figure 19 B shows more spherical and uniform sizes however, there were a few particles much larger than most. When measuring the sample with PCS the various sizes present

in the sample suspension leads to the average particle size to be inconsistent and not provide a size for the particles of interest. It was therefore important to take TEM images to fully visualise the way particles are arranged, how big the majority of particles are and what shape they have.

3.1.2 Silica-Dye Nanoparticles

Besides showing distinct fluorescent properties, compared to silica nanoparticles, silica-dye nanoparticles showed no significant differences in shape and size as seen in Figure 18.

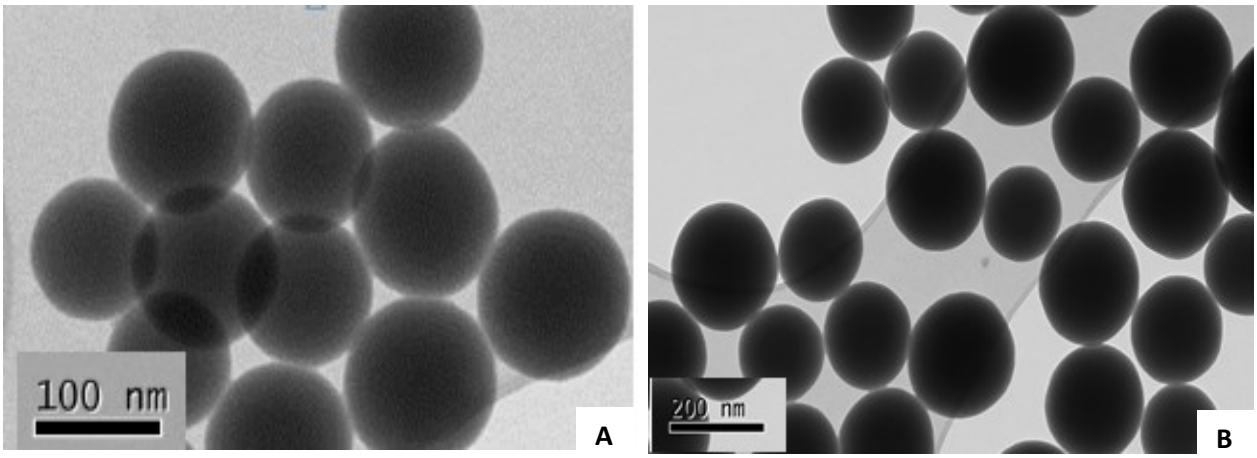

Figure 20. TEM image of Silica-Dye nanoparticles synthesised under different conditions.

Figure 20 A shows silica-dye nanoparticles that appear to be no different to particles without dye. Figure 20 B however, shows a sample where the particles have grown much larger. Although the amounts of reagents are no different, because the method of using an APS-dye conjugate alongside the normal silica polymerisation reaction slight differences can have a large effect on particle size and quality. In this case, it is likely the monomer in which the conjugate has integrated into the reaction caused the nucleation stage of the process to stop prematurely therefore fewer larger particles opposed to many smaller particles. Many factors can cause alterations including

temperature, amount of catalyst and concentration of reagents. Use of dirty or rough glassware or impure, poor quality, reagents can cause polydisperse and unpredictable particles and sizes. When preparing a sample it is therefore vital to use exactly the same method with the same reagents and the same glassware, ensuring variation of results minimised and chance of reproducibility maximised.

3.1.3 Gold Nanoparticle Synthesis

Gold nanoparticles were prepared using the method described section 2.1.3. PCS was not, however, useful in sizing the particles due to the plasmon properties and absorbance of nanosized gold. This resulted in peaks as exemplified below in Figure 21.

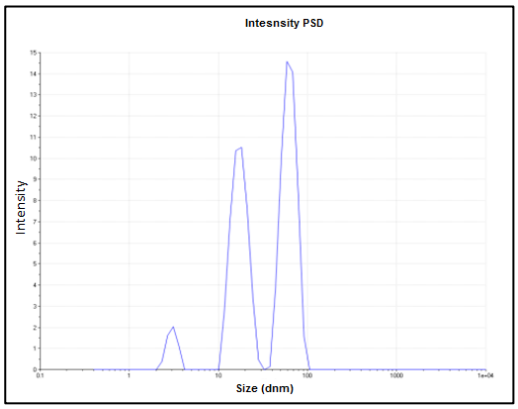

Peak 1	Peak 2	Peak 3
3.04nm (5.1%)	17.47nm (42.3%)	62.7nm (52.5%)

Figure 21. PCS results for gold nanoparticles.

It is likely the PCS is incorrectly measuring particle size since according to the literature, particle size should only range between 10-15nm. It should be noted that most published studies no not rely on PCS to measure the size of gold nanoparticles, but rather assume the size from the method of fabrication or use more direct imaging techniques such as SEM and TEM.

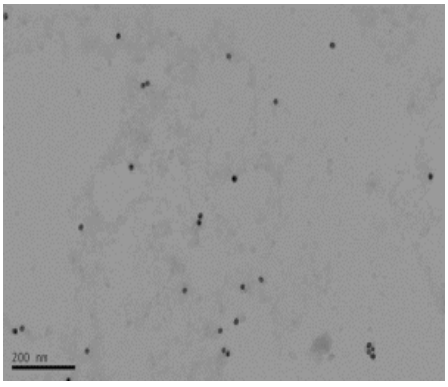

Figure 22. TEM image of gold nanoparticles surrounded by silica.

Figure 22 shows gold nanoparticles surrounded by silica, in the case of this sample the coating process was unsuccessful. However, is does provide a good image for viewing the size, shape and distribution of gold nanoparticles. They are all of similar size approximately 10-15 nm in diameter as expected, and do not appear to have coagulated, although some have formed clusters with small gaps in between.

3.1.4 Gold Core Silica Shell Nanoparticles

The initial methods for producing gold core-silica shell nanoparticles were successful, however, not all the particles possessed a gold core, shown in Figure 23.

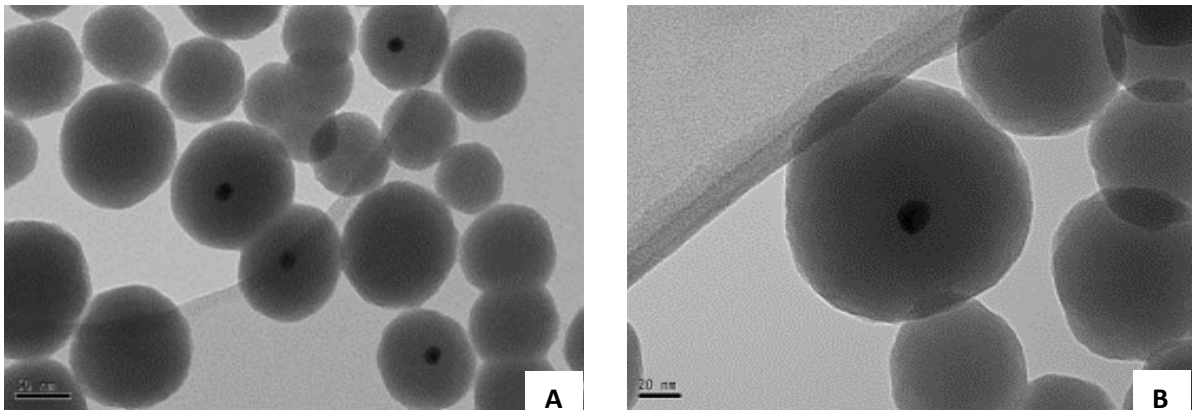

Figure 23. TEM image of gold core silica shell nanoparticles. Image A shows nanoparticles at a lower magnification including those of many different sizes and some not containing a gold core at all. B is a higher magnification image of a single gold core silica shell nanoparticles.

From these TEM images some conclusions can be drawn relating to why the method was unsuccessful. It is clear that the ratio of gold particles to the amount of silica was too small causing in silica particles to nucleate themselves and form new particles opposed to growing on the gold surface. Figure 22 A is a less magnified image and shows no evidence of gold particles not being

coated, which is one possibility. The next methods would require investigating the correct ratio of gold to silica to ensure all particles possess a gold core.

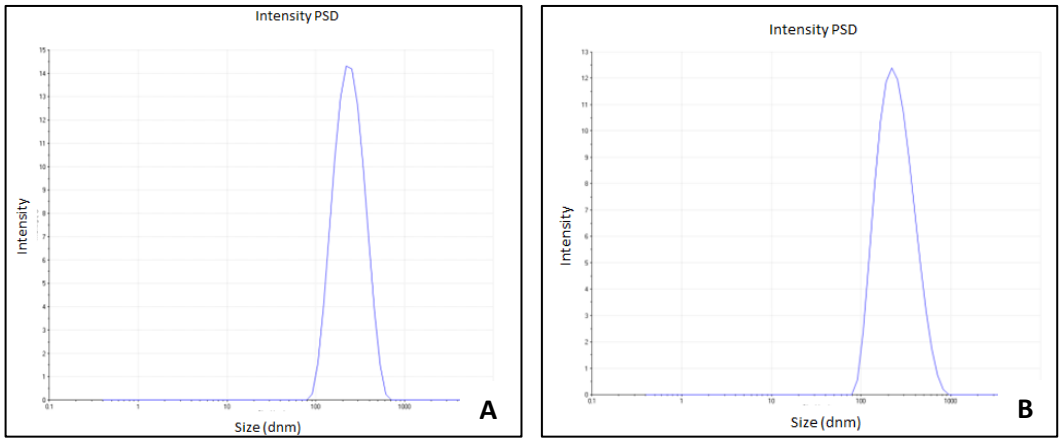

Sample Name	Peak 1
Au core SiO_2 shell (A)	252 nm (100%)
Au core SiO_2 shell (B)	265 nm (100%)

Figure 24. PCS Results for Gold Core nanoparticles.

Figure 24 shows the PCS results for the gold core nanoparticle samples. They appear to be much larger than indicated from the TEM images. This is due to aggregating of particles make the test conditions used which resulted in over estimation of particle size. It is likely the PDI is large due to the multiple sizes evident and particle aggregation.

Additional time was not spent on producing better quality particles since that was not the primary aim of the project.

3.1.5 Gold Core Silica-Dye Shell

This part of the project aimed to produce gold core silica-dye shell nanoparticles that could later be used in photocatalytic testing. The aim was to encapsulate a dye and have the plasmon boosting effect of gold boost the fluorescent signal.

Initial methods of fabricating the nanoparticle were unsuccessful as seen by the following TEM images.

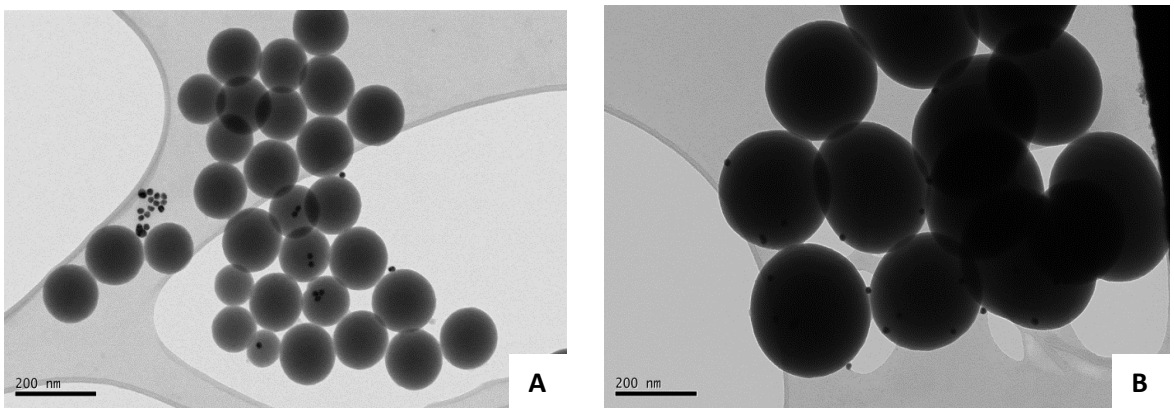

Figure 25. TEM images of gold core silica-dye shell nanoparticles.

In Figure 25 it is clear that the silica-dye had difficulty coating the gold nanoparticles resulting in large silica nanoparticles being formed without a gold core. Figure 25 A shows a cluster of gold particles indicating that there was not a lack of gold particles in this case but that the silica was unable to coat them. Figure 25 B shows gold nanoparticles only on the surface. This is likely to be due to the silica not being able to interact with the PVP gold surface. The adsorption of PVP onto the gold particles was intended to prevent aggregation via steric stabilisation. This is only a short term solution as the PVP steric bonds eventually tangle, covering the gold surface resulting in particles coagulating and preventing silica attachment on the gold surface evident by the cluster forming in Figure 25 A. In the case of this reaction the freshly stabilised PVP gold where either not used fast enough or compression by the centrifuge caused the particles to coagulate prematurely.

Centrifuging PVP stabilised gold is risky as excess PVP will interrupt formation of the shell coating, however, the process causes unwanted compression and loss of a large amount of gold particles when used under a slower setting. A method to minimise compression using a slower centrifuge setting, with vigorous sonication to disperse the particles was eventually used.

After the previous samples were examined, the method of using NaOH was introduced[40] to see if a new approach could reliably produce good, quality particles.

Table 7. PCS results for samples produced by the NaOH method.

Sample Name	**Peak 1 (nm)**	**Peak 2 (nm)**	**PDI (nm)**
MA-NP-29/03	71.0 nm (1.2 %)	540 nm (98 %)	0.653
MA-NP-1-03/04	234 nm (84.6 %)	5380 nm (15.4 %)	0.401
MA-NP-2-03/04	370 nm (78.2 %)	4950 nm (21.8 %)	0.423
NP-MA-11/04	172 nm (96.3 %)	4430 nm (3.7 %)	0.259
NP-MA-27/04	9.30 nm (8 %)	182 nm (92 %)	0.266
NP-MA-16/05	286 nm (97 %)	5560 nm (3.0 %)	0.447
MA-NP-21/05	177 nm (11.3 %)	427 nm (88.7 %)	0.796
$MaSiO_2NP1$	63.4 nm (81 %)	4.89 nm (18.9 %)	1.00
$MASiO_2RhBNP3$	69.6 nm (100 %)		0.398

Table 7 shows the PCS results for particles produced using the NaOH method. The results vary because of the different methods used. The most notable data however is that almost all the samples displayed two distinct peaks. This means that the method was unreliable in terms of producing uniform sized particles. Such high possibility of producing a polydisperse sample is evident in the PDI results where none of the samples were below the 0.07 threshold for uniformity and one sample showed a result of 1, the maximum PDI measurable. From the method used it is also apparent that the concentrations of reagents used are very small. This is a reflection of the

Kobayashi's paper where the concentrations were also small making large amounts of nanoparticles difficult, requiring very large volumes.

Although the method produced small amounts of polydisperse samples, the TEM results show that the reaction was successful at coating gold nanoparticles.

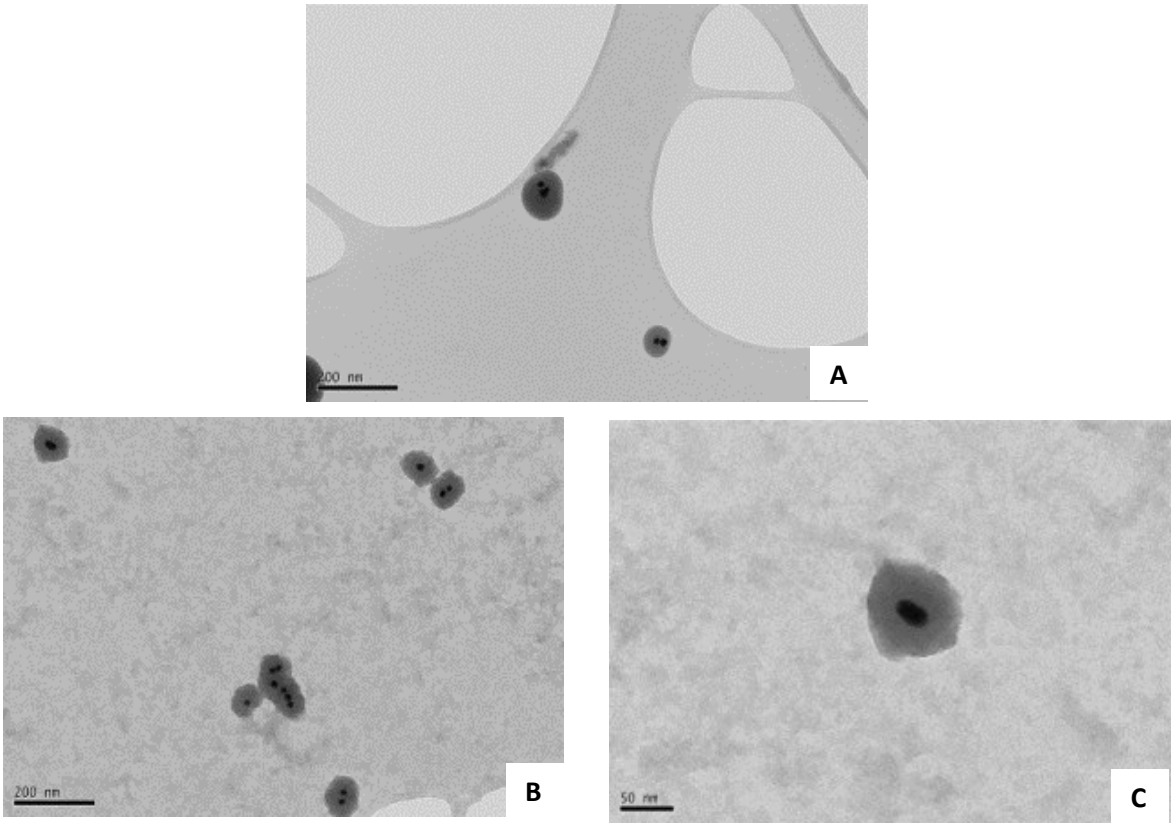

Figure 26. TEM images of gold core silica-dye shell particles produced by the NaOH method. A shows two double nuclei nanoparticles, B shows particles fused together and C shows a high magnification image of a single gold core shell nanoparticle.

Figure 26 A shows multi core particles coated in silica-dye. The multi core in this case is likely due to gold nanoparticles beginning to coagulate during formation of the shell layer. In this sample the particles where very few in number, due to change in production method. The ratio of gold to silica may also be too high, however, this cannot be confirmed. Figure 26 B shows more multi-core particles, however, the gold particles do not appear to have coagulated, showing discernible spacing between them. The particles may be linked by PVP during adsorption onto multiple particles however it is also likely the coating process occurred at a much faster rate, causing it to envelop the

loose cluster of gold particles. There is also a lot of excess silica in the suspension that should have polymerised onto the particles. This silica has instead formed silica gel, again due to the reaction occurring too rapidly. Other than producing multi-core particles and causing the silica to form gel the method was successful in producing some particles of the desired size and shape as seen in Figure 26 C.

3.1.6 Silica Core Gold Nanoshell Particles

Three silica nanoparticle samples where produced using the Stöber method for use in coating in a Nanoshell.

Table 8. Summary of the Sizes of Silica-Dye Nanoparticles for use in Nanoshell Formation.

Sample Name	Amount of TEOS (ml)	Diameter nm	PDI	Zeta Potential (mV)	APS mod zeta (mV)
SIO2RHB4	1.5	605	0.591	-64.7	17.3
SI02RHB6	1.5	631	0.059		
SIO2RHB7	1.0	220	0.122		

Table 8 shows the amount of TEOS used in each sample. They were increased from the original method in order to produce a high concentration of particles. This however resulted in increased particle size with more variation in the quality of particles. SIO2RHB4 was reacted in a conical flask while SIO2RHB6 used a round bottomed flask. The round bottomed flask provided a far better reaction environment for producing nanoparticles in terms of producing high levels of monodispersity. The PDI of SIO2RHB6 is significantly lower than SIO2RHB4 and being below the 0.07 threshold it is considered monodisperse. The amount of TEOS affected the size significantly, as seen by a decrease of 0.5 ml in SIO2RHB7. Although not as monodisperse, the sample was of sufficient quality for coating, but more importantly it was of a more suitable size as smaller particles would

provide an improved surface area to volume ratio. Zeta potential was measured for the first sample during APS functionalization. Initially the zeta potential is negative due to the surface silica creating a repulsion force between particles; by adding APS to the surface amine bonds will become more frequent, shifting the potential to a more positive state. The zeta potential reading indicates that a large amount of the surface had been functionalised resulting in an overall positive surface potential. It is important to maintain a high surface potential in order for the sample to remain stable due to repulsion forces preventing particles from naturally coagulating. Logically more APS would lead to more surface modification and therefore a more stable product. APS is however capable of polymerising in the presence of oxygen, although the synthesis can be performed under nitrogen there is no guarantee so as little APS was used as possible to prevent contamination.

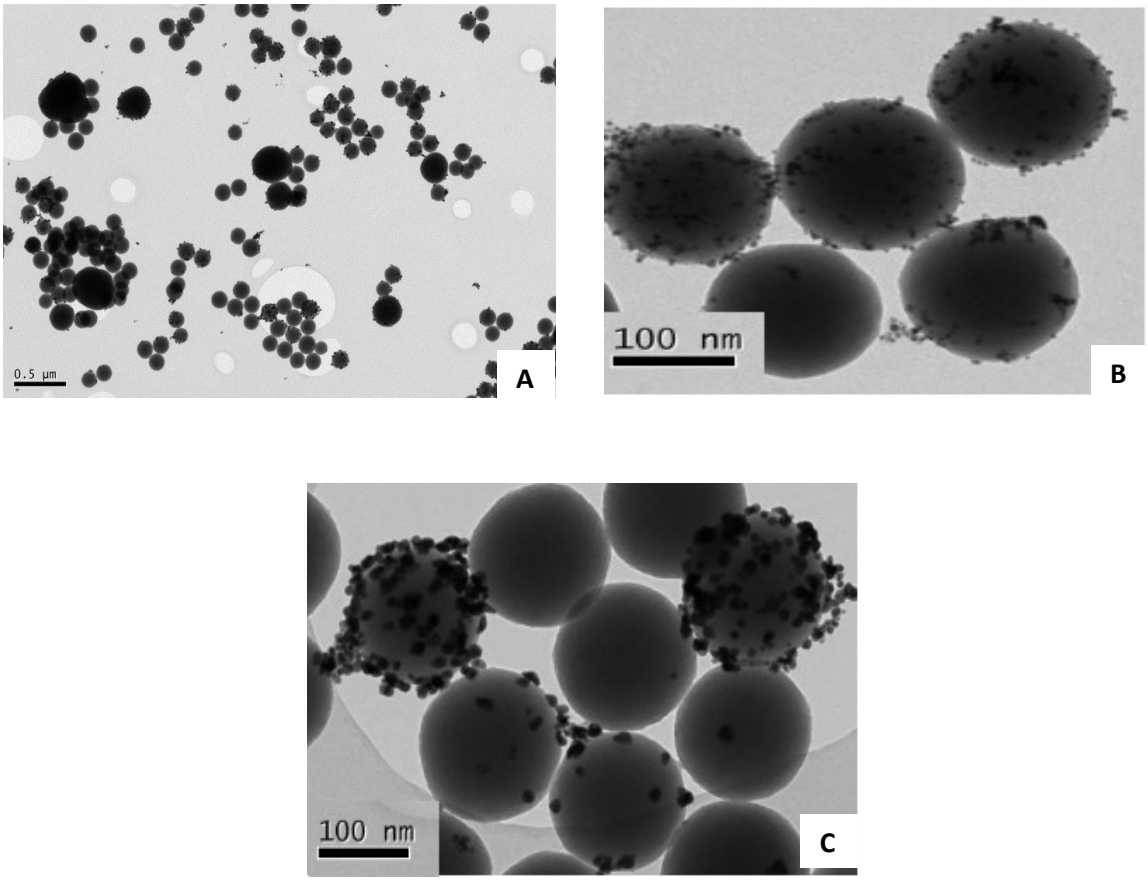

Figure 27. TEM images of silica-dye particles coated in gold seeds.

Figure 27 shows TEM images of silica-dye nanoparticles coated in gold seeds. The PCS results indicated it was not monodisperse with a PDI of 0.122, which is clear from the larger particles dotted about the Figure 27 A. The attachment of gold seeds is not complete either (Figure 27 B and C) where some particles have some gold and others have little or none. There are some possible explanations to this effect. The initial APS functionalization was insufficient, leaving some particles not coated in APS at all. It is therefore likely that APS in the functionalization stage is required or that the reaction should be continued for longer. Without APS functionalization the gold seeds could not bind to the silica shell. This is unlikely to be the only contributing factor as there would still be an even distribution of APS on each particle and therefore an even amount of gold on each particle. The reason for the uneven distribution is caused by the method used for adding gold seeds to the functionalised particles. The method added a fixed amount of gold and vortexing to mix. The method required the particles to remain static for binding to take place, however, this caused some particles to acquire more gold than others and likely needed gentle mixing for a longer period of time to ensure the particles bind on the surface and for a more even distribution.

Figure 27 C is interesting as it has larger gold seeds on the surface. This change is caused by the use of hydroxylamine hydrochloride in combination with gold salt to build up a gold shell. This method essentially adds gold atoms to the gold seeds eventually causing them to fuse together to form a shell. The shell formation was not complete as it was stopped after a colour change from a rust brown to navy blue was observed. The change indicated that the seeds became bigger and fusing together. This fusion resulted in loss of the ruby red colour, which is indicative of the presence of gold nanoparticles.

Note that PCS was not performed on particles after the addition of gold due to the plasmon effect, which adversely affects the accuracy of size measurements. PCS was not carried out either as the particle size should not change during the gold seed addition reaction.

3.2 Fluorescent enhancement

One of the primary aims of this project was to demonstrate the plasmon boosting effect of gold nanoparticles in enhancing fluorescent dye, of which rhodamine B was chosen to be suitable. In the nanoparticle synthesis stage particles where made demonstrating possible methods of plasmon boosting, via a gold core coated in a silica-dye shell, a silica-dye core coated in gold seeds and a silica-dye core coated in a gold shell. Fluorescence was performed on each sample and compared with silica-dye nanoparticles containing the equivalent number of dye molecules (9.66 x 10^{20} molecules).

3.2.1 Gold Core Silica-Dye Shell

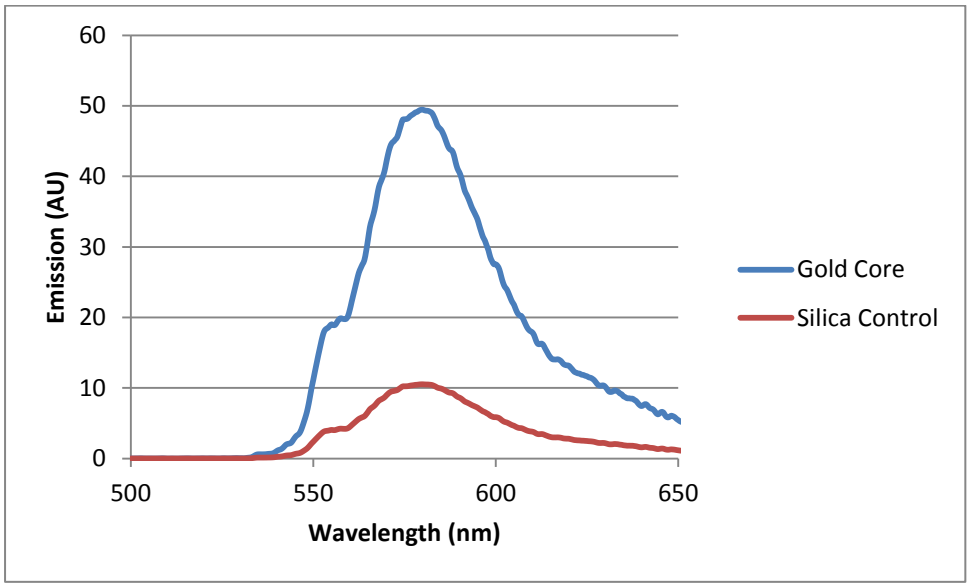

Figure 28. Fluorescence spectra showing the enhancement of gold core nanoparticle (B) compared to one silica-dye control (A).

Figure 28 shows a fluorescence spectra of a gold core silica-dye nanoparticle compared with a silica-dye nanoparticle, both samples containing the same amount of dye and therefore should produce the same fluorescence. The gold core sample however produced, significantly more fluorescence

than the control by a factor of 4.9 (peak of 48.8 ÷10.2). This result demonstrated what was to be expected from the literature. In possessing a gold core the plasmons on the surface were capable of boosting fluorescence interactions of the dye within the silica shell. This resulted in a more efficient fluorescence interaction providing an amplified emission signal. This was only a basic test to see if there was any affect at all, the exact level of enhancement would require additional, testing.

3.2.2 Silica-Dye Core Gold Shell (C)

The gold nanoshell consisted of a silica-dye nanoparticle coated with gold seeds with the addition of a gold salt and hydroxylamine hydrochloride in order to add additional gold to the seeds, such that they gradually fuse to form a shell. The following graph compared the fluorescence properties of a silica-dye nanoparticle and one coated with a gold nanoshell containing the same number of dye molecules (9.66 x 10^{20} molecules)

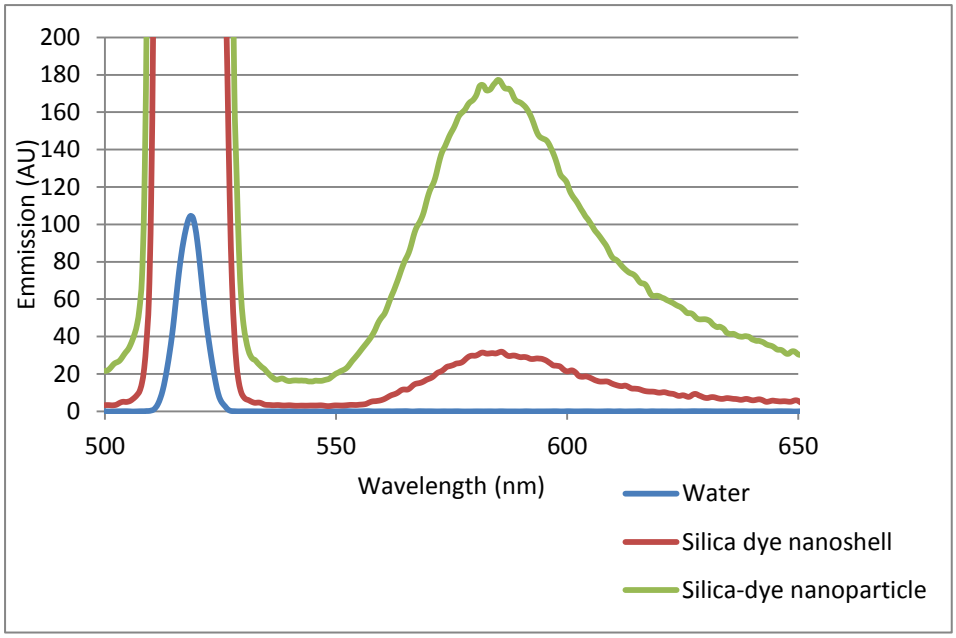

Figure 29. Fluorescence Spectra of Silica-dye nanoparticles and Nanoparticles Coated in a Nanoshell.

Unlike the gold core nanoparticle in Figure 28, the gold nanoshell did not produce the same boosting effect as seen in figure 29. The graph shows that a basic silica-dye nanoparticle has peak fluorescence at 174.6, whilst with a gold shell this is reduced to 31.3. This is likely due to the gold nanoshell on the surface not exhibiting the same plasmon boosting properties normally seen in nanosized gold. This loss was observed when the mixture changed in colour from a rust red to navy blue as a result of further addition of gold. The rust red colour is caused by the plasmons on the gold nanoparticle surface absorbing light to give a red colour, when fused with other gold seeds the plasmons change their resonance wavelength further towards the infrared resulting in a loss of colour changes. The nanoshell is no longer in a position to enhance fluorescence of rhodamine B dye (580 nm absorbance), but instead interferes with light entering and exiting the nanoparticle effectively reducing the fluorescent signal even though the same amount of fluorescent molecules (rhodamine B dye) were present (Figure 30). This is evident in the literature where nanoshells are used to enhance plasmon resonance in the infra-red opposed to fluorescent dyes[21].

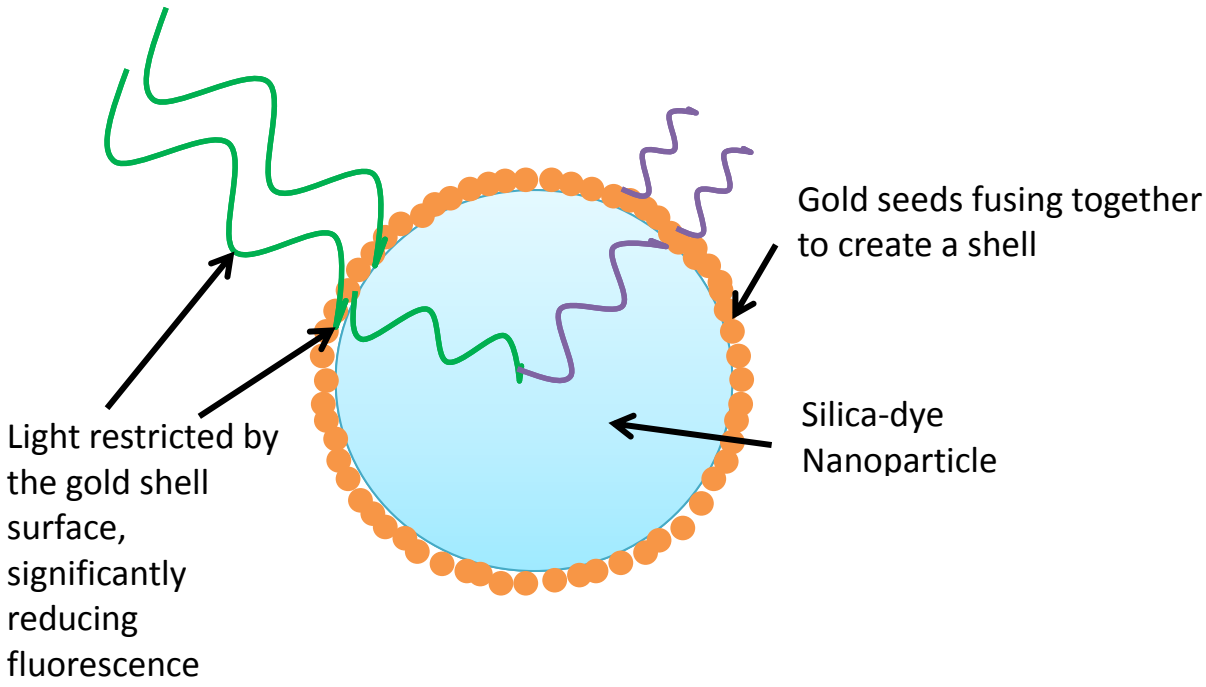

Figure 30. Diagram representing the effect of a nanoshell on a silica-dye nanoparticle fluorescence.

This result was once again to gain a basic level of enhancement or loss of fluorescence. Additional testing is required to calculate a more accurate level of fluorescent loss.

3.2.3 Silica-Dye Core Coated in Gold Seeds Nanoparticles (D).

Silica-dye nanoparticles coated in gold seeds were compared with silica-dye nanoparticles for their fluorescent properties containing the same number of dye molecules (9.66 x 10^{20} molecules)

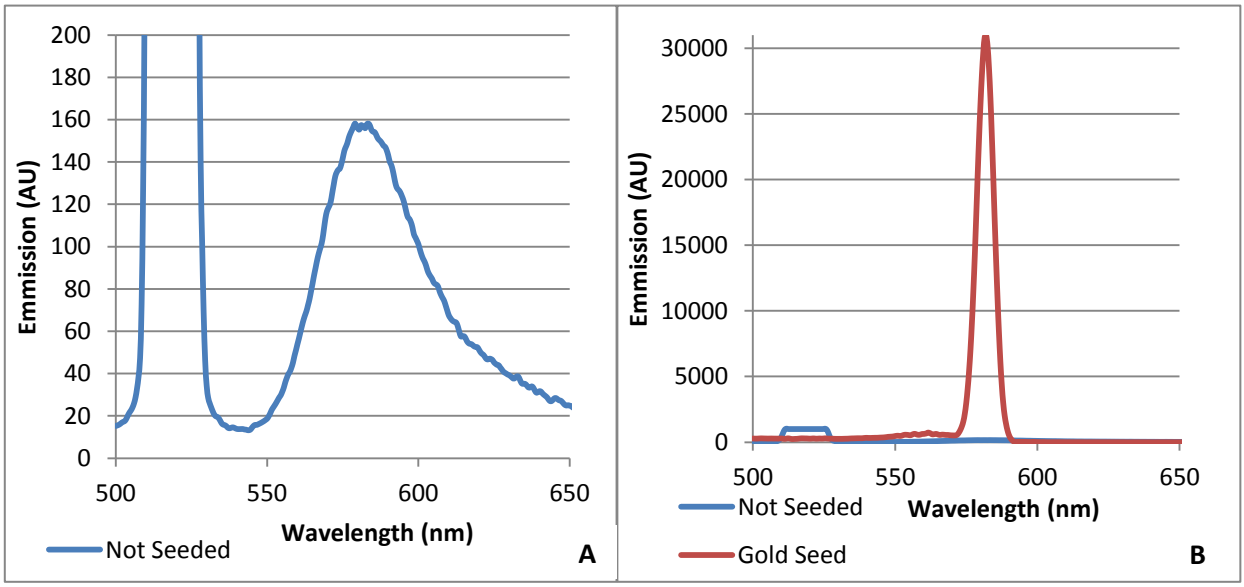

Figure 31. Fluorescence comparison of silica-dye control (Particle A) shown in graph A and silica-dye coated in gold seeds (Particle C) shown in graph B.

Figure 31 A shows the fluorescence emission of silica-dye nanoparticles without any gold seeds. The peak reaches only 157 AU. Figure 31 B shows the fluorescence emission of silica-dye coated in gold seeds compared to the control. The gold seed sample has a peak of 3 x 10^4 AU. Both samples contained the same amount of rhodamine B molecules so any change in fluorescence was caused by light interacting with gold seeds and their surface plasmons. Using the values from the graph, the introduction of gold seeds resulted in a 196 fold boost in fluorescence. This is a significant difference in activity relative to the gold core, which only gave a 4.98 fold increase in activity. Therefore there

are factors that have allowed plasmon boosting they occur more effectively. To gain an accurate level of fluorescence enhancement more testing is required.

In the gold core nanoparticle, the plasmon boosting only effects dye molecules in a certain radius with the maximum effect located 25nm from the gold surface. This is shown in Figure 30.

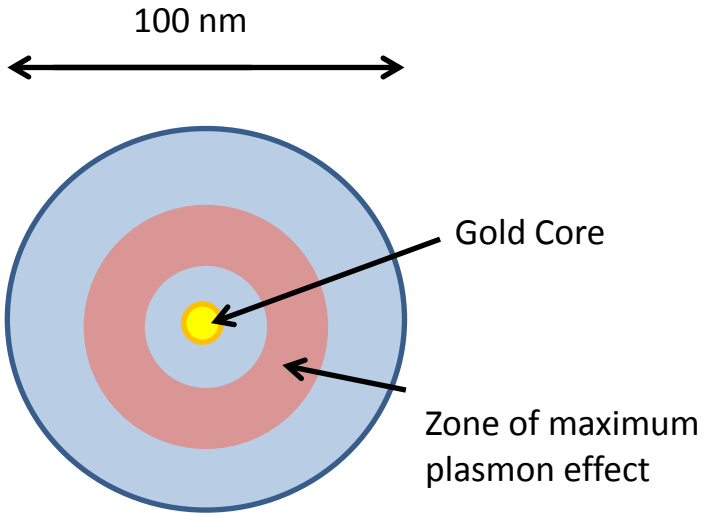

Figure 32. Diagram representing the area of plasmon boosting in a gold core silica-dye nanoparticle.

The area of maximum plasmon effect is the area in which the plasmons emitting from gold boosts fluorescence. In Figure 32 the core in the centre provides only one surface for plasmon emission, limiting the amount of plasmons available for fluorescence boosting. The zone of maximum plasmon effect is also well within the nanoparticle where only a fraction of the light used for possible fluorescence can penetrate. This is a major factor as the majority of fluorescence will occur on or near the nanoparticle surface and only a small amount deeper in. It is possible to make a thinner shell however, which does improve the signal[40].

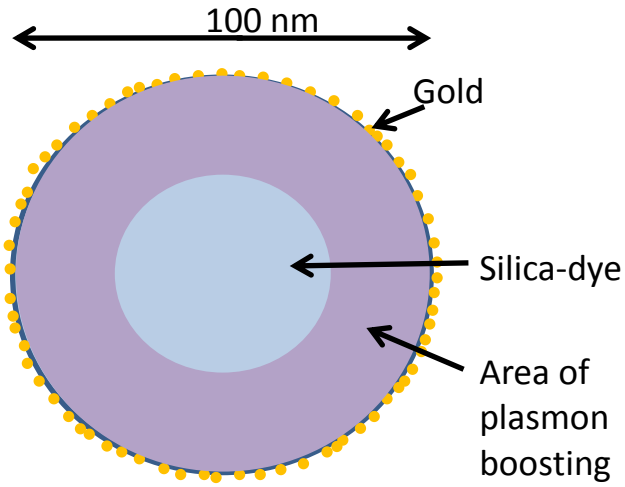

Figure 33. Diagram representing the area of plasmon boosting for a silica-dye nanoparticle coated in gold seeds.

Figure 33 shows that the area of plasmon boosting is much larger due to the gold seeds being present on the surface. This also allows for plasmon boosting to occur in the area where light will be most abundant. As there are many gold seeds with their own plasmon cloud, opposed to a single core producing one cloud. The area of plasmon boosting contains significantly more plasmons, they further enhancing the fluorescent properties of rhodamine B in this area. The benefit of this method is that the size of the nanoparticle is not very critical in terms of boosting dye molecules. The benefit of smaller particles would provide a better surface area to volume ratio and reduce the number/fraction of dye molecules which are not within the plasmon cloud.

One part of the model that cannot be explained is that normally fluorescent interactions so close to a gold nanoparticle are self-quenched, which means that photons emitted from dye molecules are absorbed by the gold nanoparticle itself. This could still be occurring and the other factors are overriding this, however, with the scope of this project it was not able to quantify and explain this.

3.3 Titanium Dioxide Film

3.3.1 Step thickness measurements

Table 9. Step thickness results for sputtered films.

Sample name	**Thickness (µm)**	**Standard Deviation**
TiO_2 20/01/12	-	-
TiO_2 24/01/12	0.555	0.014
TiO_2 25/01/12	1.086	0.012
TiO_2 26/01/12	1.01	0.014
TiO_2 30/01/12	1.06	0.161
TiO_2 03/02/12 (1)	2.205	0.114
TiO_2 03/02/12 (2)	2.356	0.010
TiO_2 03/02/12 (3)	2.314	0.005
TiO_2 08/02/12	-	
TiO_2 10/02/12	-	
TiO_2 15/02/12 (1)	1.798	0.026
TiO_2 15/02/12 (2)	1.973	0.508

Table 9 shows how the TiO_2 films varied in thickness. The results were acquired by measuring six different steps in different areas of the film and finding the average. Six different measurements are deep accurate enough for a reliable average thickness since there should be no large variants on a stable film. There is an increase from sample TiO_2 24/01/12 to TiO_2 26/01/12 since this is where the reaction time was increased to 100 minutes to create a film 1 µm thick, which was successful. The three samples prepared on 03/02/12 where all much thicker due to use of a much lower sputtering

frequency. This allowed more TiO_2 to deposit in one cycle rather than smaller amounts more frequently. This method produced a much thicker film. The final two films where thicker than those performed before 03/02/12 since they used a longer deposition time of 120 minutes but the same frequency. Films with no thickness results stressed during or after sputtering causing the film to peel off and become immeasurable. The reason for this was often due to inconsistencies in the reactive gas flow, leading to irregular rates of TiO_2 deposition that did not form a quality film.

3.3.2 Raman Spectra

Analysis of Raman spectra involved identifying the key peaks that should be expected to characterize the composition. In this section these peaks will be identified as different TiO_2 morphologies, whilst any other peaks identify impurities or organic interference on the surface of the film.

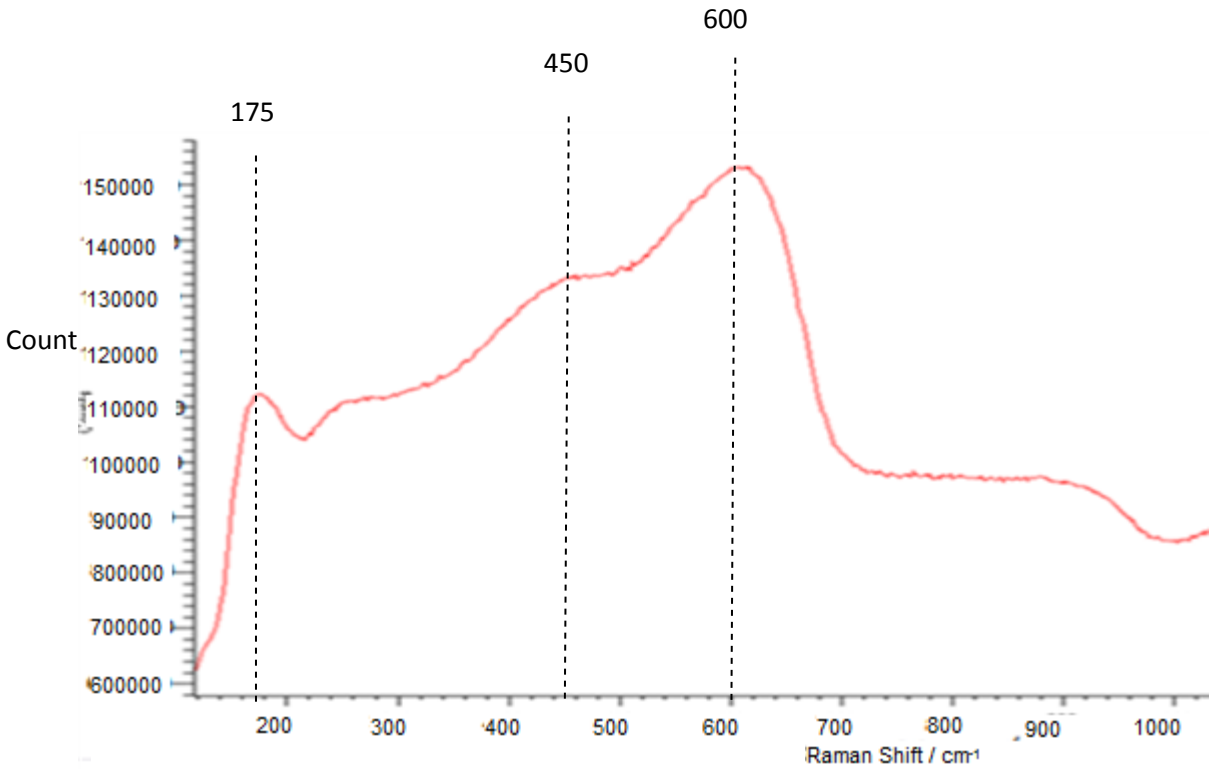

Figure 34. Raman spectra of sample 3.02.12.1, 2.205 µm thick.

Figure 34 shows a clear peak at 600 cm^{-1} and 450 cm^{-1}, therefore film mainly consists of rutile TiO_2 however, the peaks are not very sharp indicating the material may not very crystalline and instead more granular. This could be due to the angle of the laser. There is also a peak at 175 cm^{-1} indicating a small amount of the anatase form TiO_2.

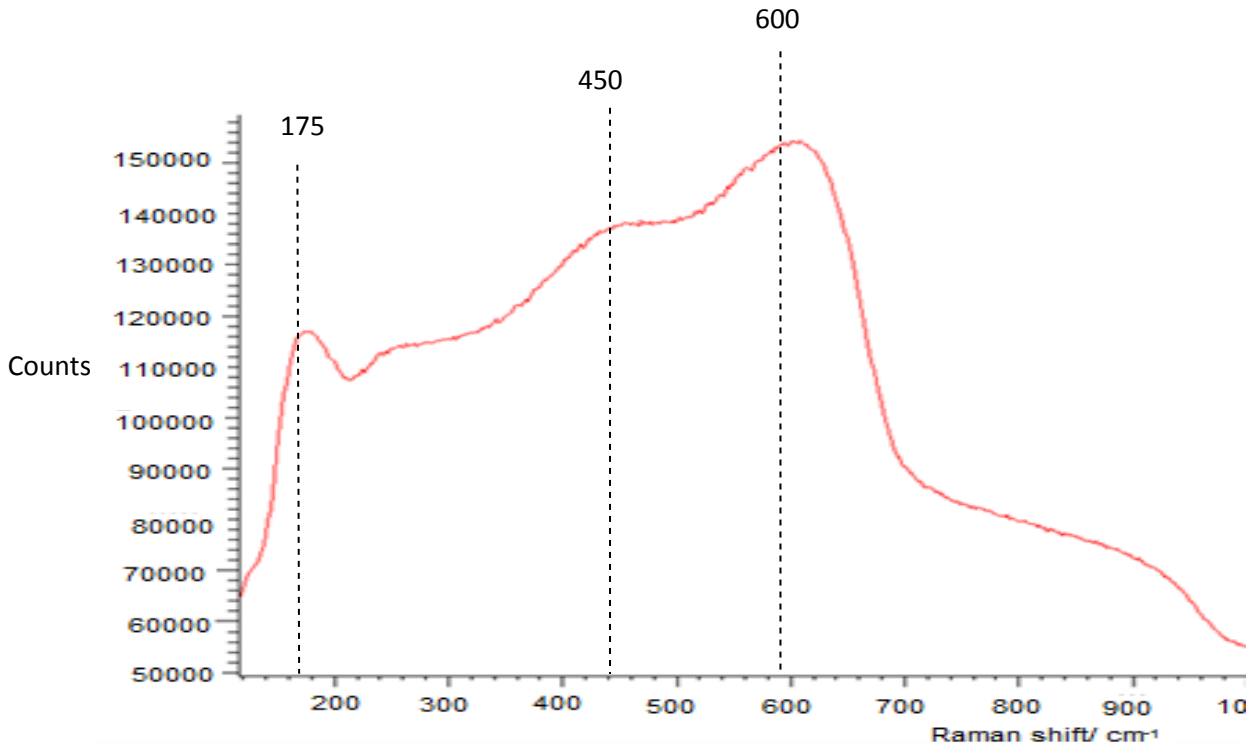

Figure 35. Raman spectra of sample 3.02.12.2, 2.356 µm thick.

Figure 35 shows a similar spectrum showing a high rutile peak at 600 cm^{-1} and 450 cm^{-1} however a small anatase peak can be seen at 175 cm^{-1}.

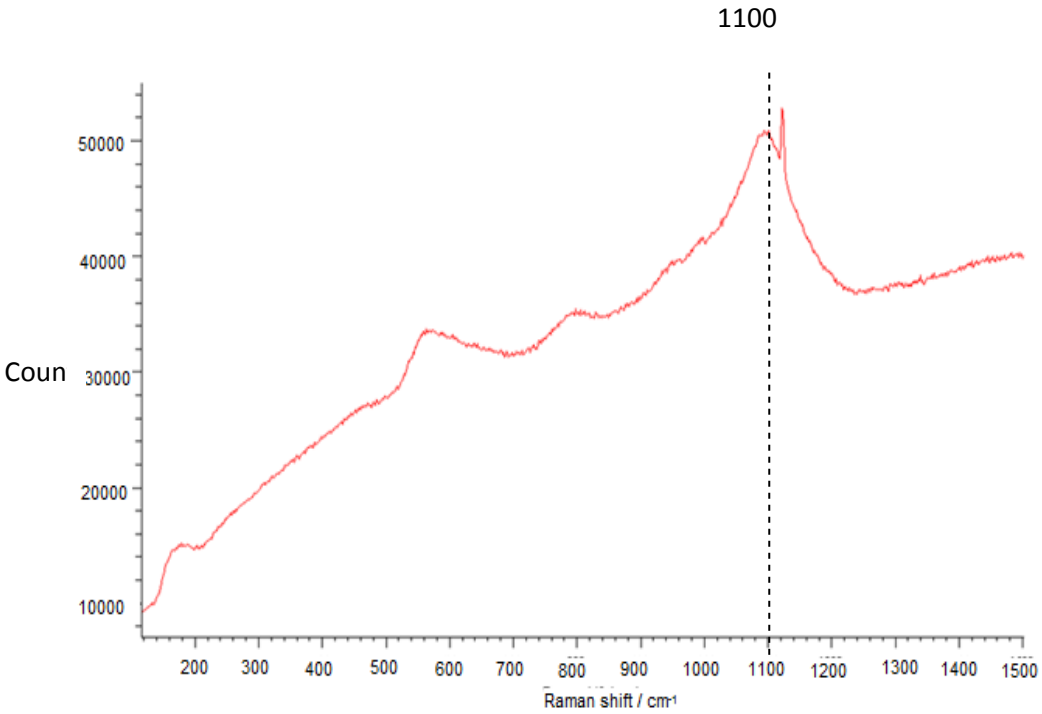

Figure 36. Raman spectra of sample 3.02.12.3, 2.314 µm thick.

Figure 36 shows a poor Raman spectrum showing none of the relevant peaks that would be seen in a TiO_2 sample. There is only one clear peak at 1100 cm^{-1} indicating the presence of organic material such as residue from touching the surface without gloves, which have likely covered the surface and masked the TiO_2 crystals.

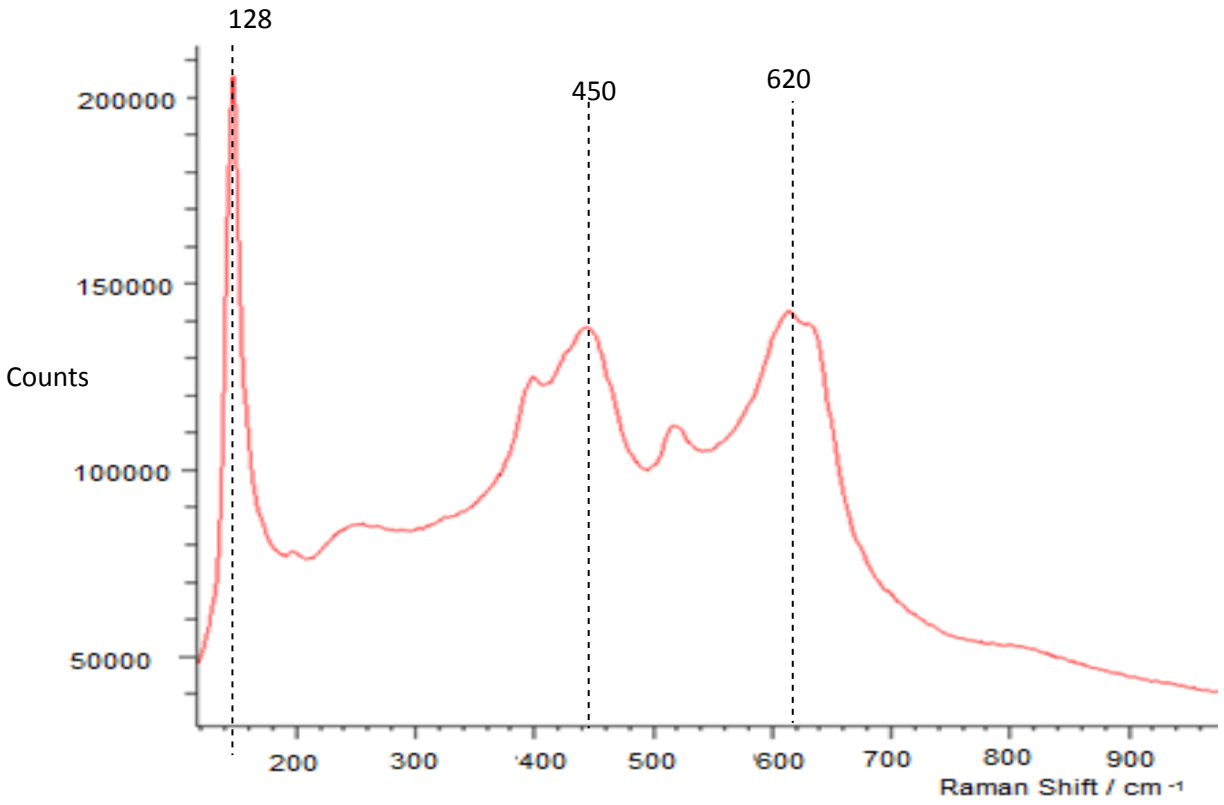

Figure 37. Raman spectra of sample 25.01.12, 1.086 µm thick.

For Figure 37, this sample has a much higher proportion of anatase by the high peak at 128 cm^{-1}. There is also some rutile forming peaks at 450 cm^{-1} and 620 cm^{-1}. This sample therefore has a mixture or crystal types, though as both anatase and rutile have strong photocatalytic properties, this sample would be expected to possess more activity that others (as described in section 1.3).

These samples show a range of different structures indicating that the sputtering conditions matter greatly in producing a high quality film. It is however, important to ensure the film is pristine when undergoing Raman spectroscopy to ensure the laser irradiates the Titania sample and not the contaminated surface. The organic contamination was likely due to poor handling during any part of the sputtering process and when undergoing Raman analysis. Excessive cleaning was avoided due to

some films being very fragile. The hardness of films was not investigated, so long as the film was intact and exhibited some photocatalytic properties it was used for further testing.

3.3.3 SEM Imaging of TiO_2 Films

SEM was used to provide a visual analytical tool for examining the surface of TiO_2 films. This provides information on crystal size, how granular/smooth the surface is and also provides possible insight into how the surface looks in relation to its composition and photocatalytic activity. All images shown are at x 50,000 magnification. This is the maximum magnification that produced a clear image.

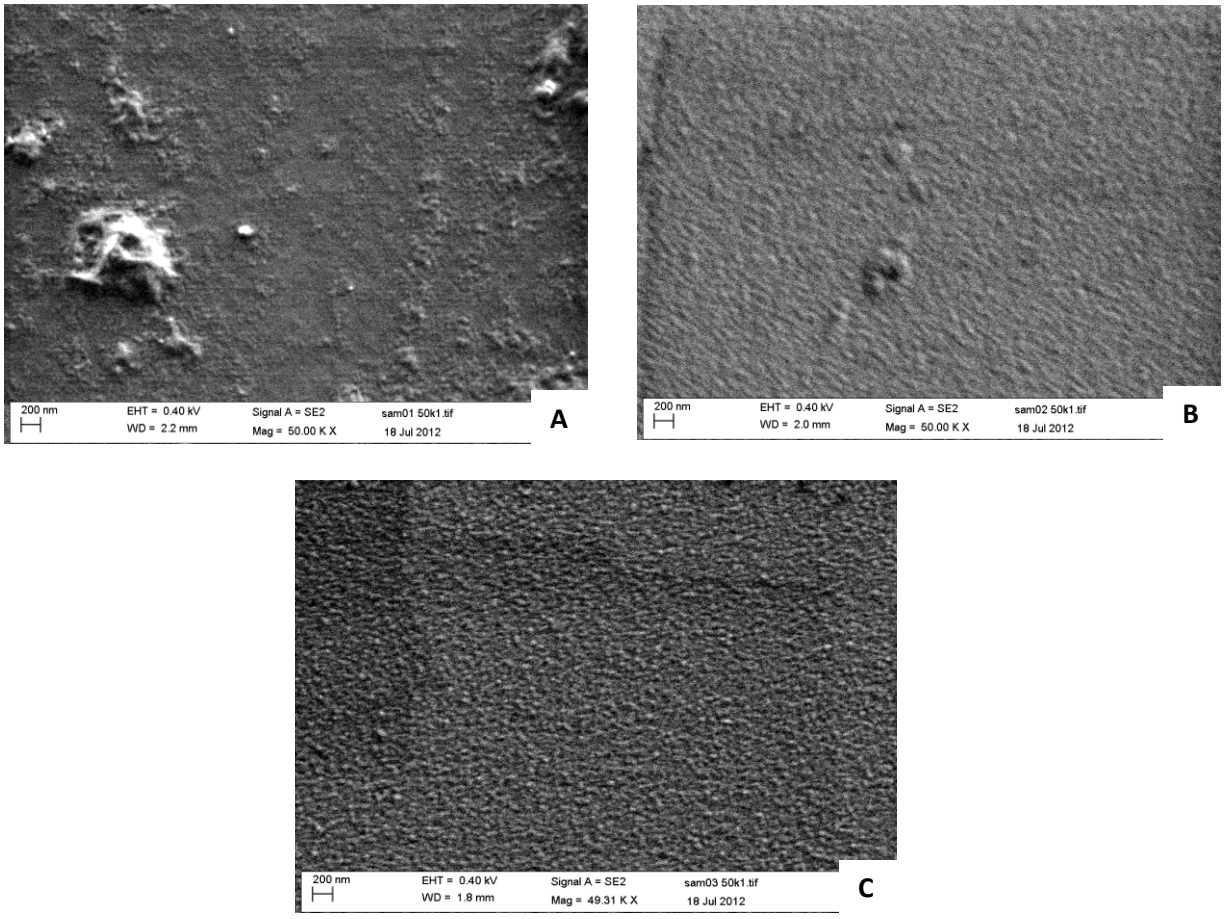

Figure 38. SEM images of sample 3.02.12.1 (A) 3.02.12.2 (B) 3.02.12.3 (C), 50k magnification.

Figure 38 shows SEM images of samples A 3.02.12.1, B 3.02.12.2 and C 3.02.12.3. Each sample shows different surface morphology, however A 3.02.12.1 and B 3.02.12.2 share similar results from the Raman analysis, with C 3.02.12.3 being very different. Interestingly these samples were all sputtered at the same time under the same conditions. From Figure 37 A it is evident that this example shows uniform surfaces with patches of granular crystals varying in size between 400 nm and 20 nm. Although varied, these crystallites increase the surface area for excitation and hence the frequency of radical formation. Figure 37 B however shows an almost completely uniform surface however, the small granules are typical of a rutile crystal, which is also confirmed by the Raman spectra. The larger granules in Figure 38 A are likely to be anatase crystal formations accounting from the small peak in the Raman spectra. For Figure 38 B however, the anatase crystals must be smaller and far more spread out such as shown in the centre of the image. Figure 38 C however, does not show any large crystal formation and appears to be a rougher but with a uniform surface. The Raman analysis of these samples showed only a high level of organic contamination however, it is likely to be primarily rutile. From the Raman spectra and SEM images it is likely these three

films are primarily rutile therefore possessing a moderate amount of photocatalytic activity however not the best.

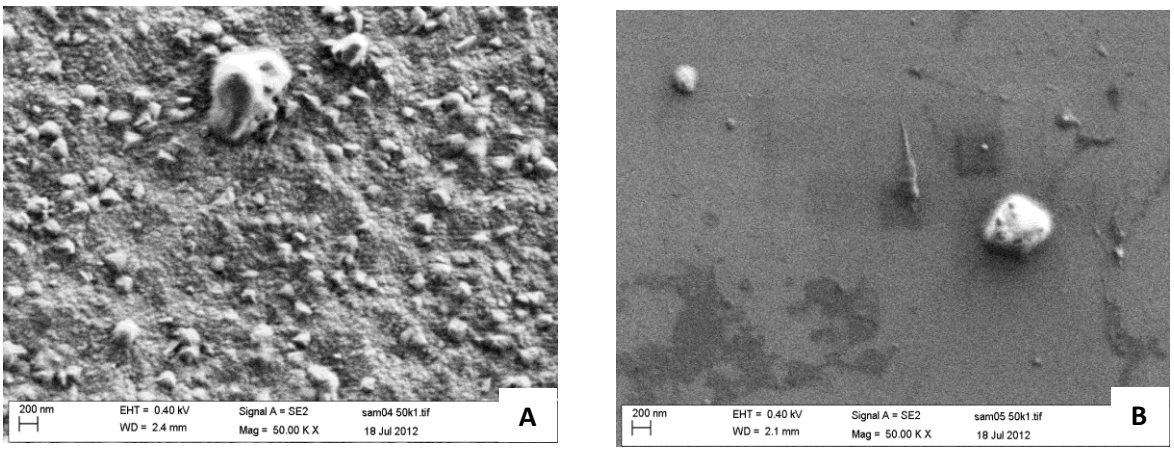

Figure 39. SEM images of samples (A) 25.01.12 (B) 26.01.12 x 50,000 magnification.

Figure 39 A shows sample 25.01.12, which showed a very high level of anatase crystals as confirmed in the Raman spectra. This becomes clearer in this SEM image where there are an abundance of anatase crystals present as opposed to just a few in Figure 38 A. This sample is likely to possess high levels of photocatalytic activity. Sample 26.01.12 however, is nearly the complete opposite with an extremely smooth surface with a few crystal formations. The Raman spectra did not however, show what this sample composed of due to high levels of organic contamination. Compared to other film samples it is likely to be a rutile film but this cannot be certain.

.

3. 4. Photocatalysis Results

To verify the excitation wavelength required the absorbance of RhB isothiocyanate was measured. This measurement coincides with the wavelength required to excite the electrons within the dye molecule. This was measured by UV-VIS spectroscopy. The peak absorbance was found to be 560 nm as seen on Figure 40 so to fluoresce the dye a light beam of 550-560 nm was used.

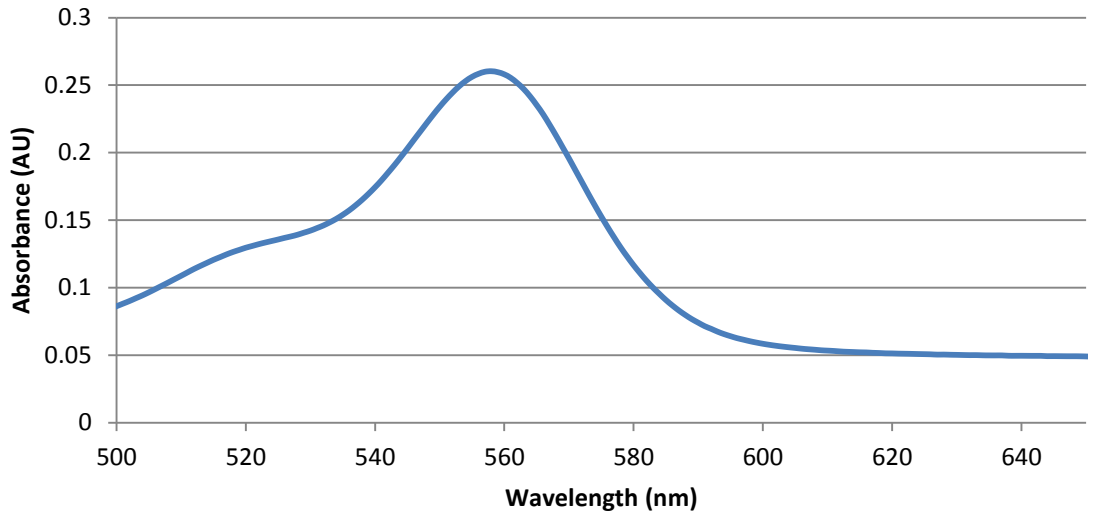

Figure 40. UV-VIS absorbance of rhodamine B isothiocyanate (9.66 x10^{20} molecules).

3.4.1 Plasmon Boosting of Photocatalysis by Gold Nanoparticles in Suspension

This section presents the results for photocatalytic breakdown of rhodamine B with a TiO_2 film under UV light with and without the addition of gold nanoparticle (9.66 x 10^{20} molecules)

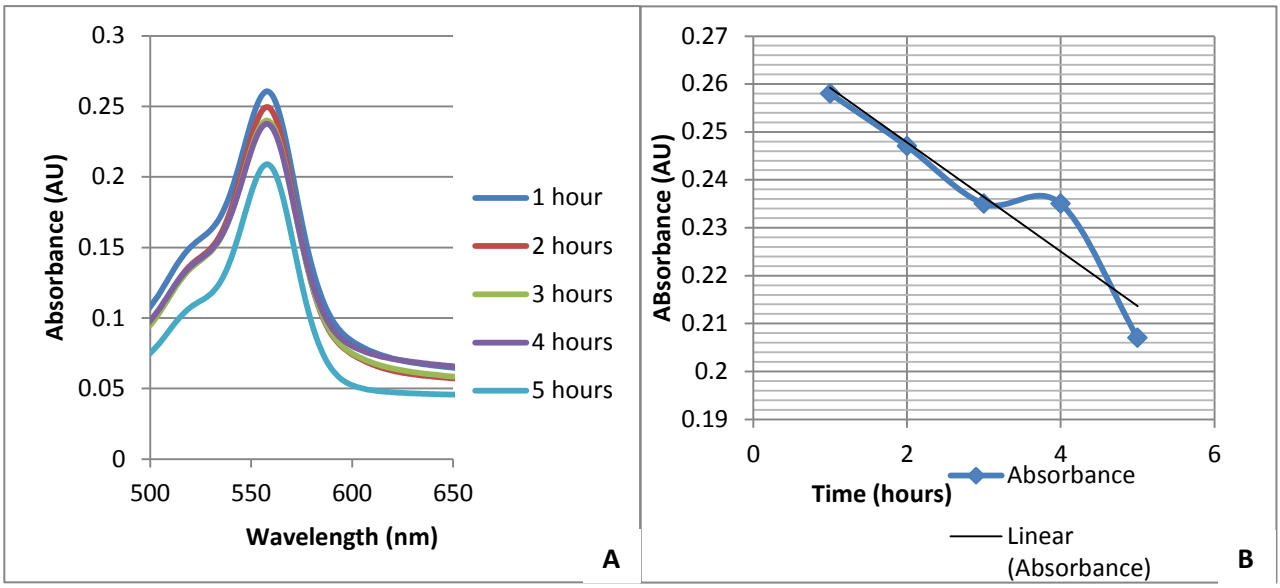

Figure 41. A, Family of UV-Vis spectra for Rhodamine B after irradiation with UV light with the addition of 2 ml Au nanoparticle suspension and B, Absorbance of 560 nm versus irradiation time.

Figure 41 A shows the absorbance spectra of RhB under UV light (360 W) in the presence of a TiO_2 film and 2 ml of gold suspension. Note that the peak for absorbance is approximately 560 nm which coincides with the initial absorbance reading. The peak absorbance at 560 nm is plotted against irradiation time (Figure 41 B) to show the decay in absorbance. The gradient of the graph is equal to the absorbance decay rate, which in the above case is 0.114 AU/hour.

The following table shows the rates of decay for the other decay experiments performed

Table 10. Decay Rates of gold enhanced photocatalytic samples.

Sample	**Decay rate (abs/hr)**
Rhodamine B control (no TiO_2 or Au)	-0.0046
Au 1	-0.0114
Au 2	-0.0105
No Au 1	-0.0056
No Au 2	-0.0047

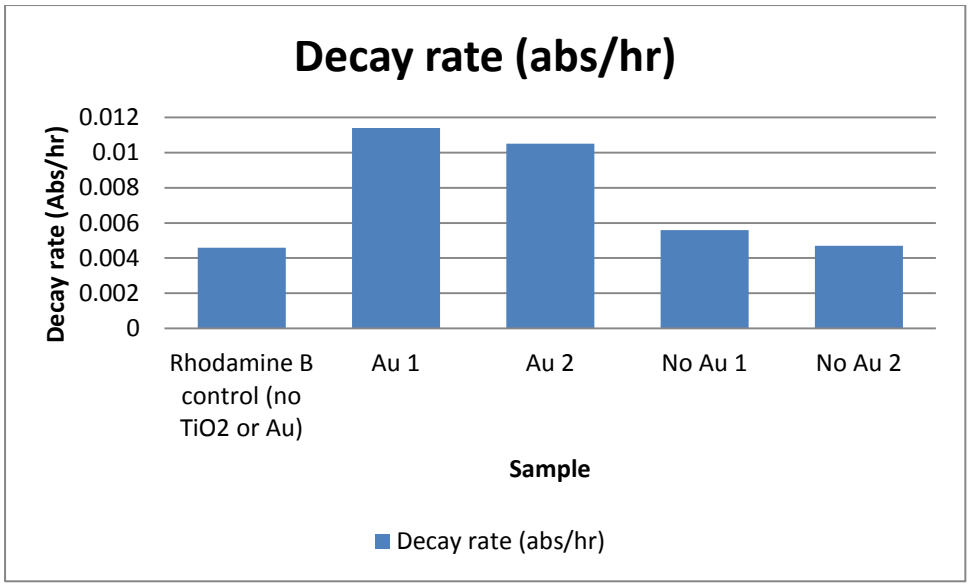

Figure 42. Bar Chart of sample decay rates.

The results from Figure 42 show that there is an effect of introducing gold nanoparticles to TiO_2 to enhance photocatalysis. By calculating the means of each set of results, the enhancement is a factor of x2.13. There was no set limit to how much gold suspension to add however, sufficient gold was added in the same range as nanoparticles contained in previous tests. Additional gold could

therefore be used and provide a greater result however, the base and maximum amount has not been investigated. It is possible to reach a saturation point where additional gold will not provide any additional effect or reduce effectiveness. Only 2 tests were performed leaving the value of enhancement inaccurate.

This coincides with current literature [20] that Au plasmon enhancement of TiO_2 photocatalysis occurs however, the results show only an x2.1 increase opposed to x66 possibly due to the different method used to introduce gold nanoparticles. The authors of reference 20 ensured a maximum effect from the gold nanoparticles by coating the surface in a 5 nm layer while in this project the gold remained in suspension and had little contact with the TiO_2 surface. The enhancement is unlikely caused by direct contact of TiO_2 and gold nanoparticles and is more likely to be due to photon enhancement, however, having gold as close to the particle surface as possible will maximise the effect. If it was possible to use a TiO_2 film that responds to wavelengths corresponding to visible light this will coincide with the absorbance of gold nanoparticles, and therefore give a greater effect.

3.4.2 Plasmon Boosting of Photocatalysis by Gold Cores and Gold Seeds

In this section data from an experiment to examine the effects of gold cores coated with a silica-dye shell (particle B) on the degradation of dye within the silica matrix (4.83 x10^{20} molecules) is reported.

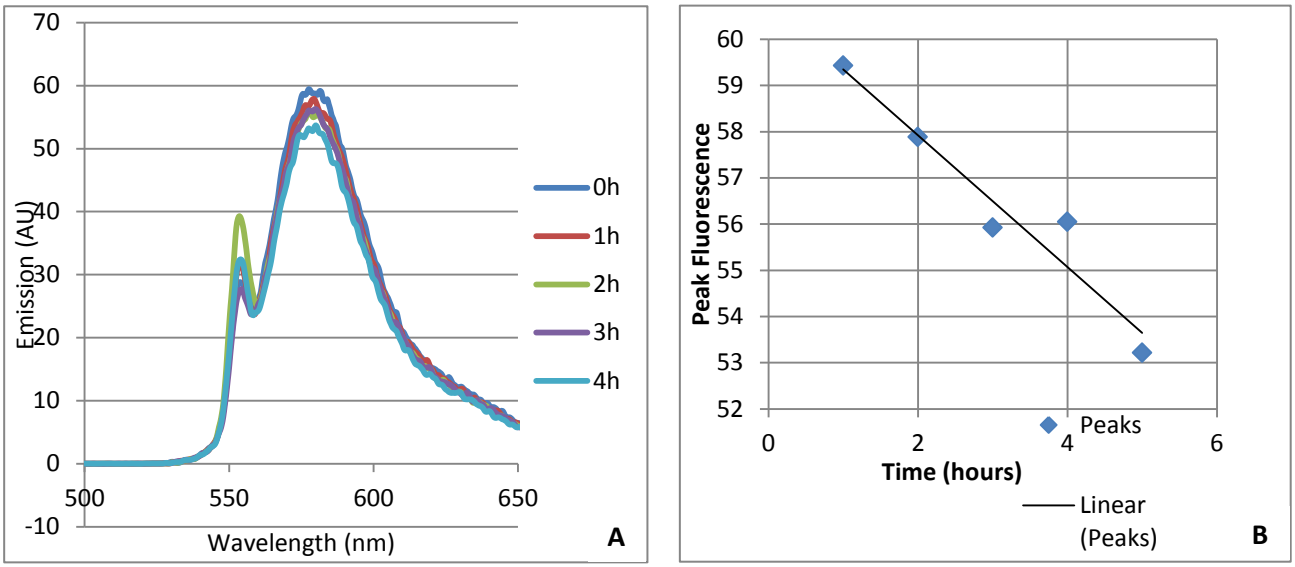

Figure 43. A, Family of Fluorescent spectra for RhB after irradiation with UV light over time (A), plot of fluorescence peak maxima against over time showing rate of degradation gradient (B)

Figure 43 A shows a family of fluorescence spectra of RhB which has been irradiated with UV light for different time periods. The peaks were measured from 560 nm and graphed against irradiation time and a line of best fit found showing a rate decrease of 1.43 AU per hour as shown by the line of best fit, with a gradient representing the rate. This shows that UV light alone causing photobleaching. The results for rates of breakdown were recorded by extrapolating the gradient in the same way.

Table 11. Results of UV irradiation over time.

Sample	**Rate of degradation (fluorescence per hour Au/hr)**
RhB in H_2O	-1.4259
RhB in H_2O with TiO_2	-2.7482
RhB+APS with TiO_2	-
SiO_2-Dye nanoparticle (A) with TiO_2 (1)	-
SiO_2-Dye nanoparticle (A) and TiO_2 (2)	-
SiO_2-Dye nanoparticle (A) and TiO_2 (3)	-
RhB encased in SiO_2 with gold core and TiO_2 (1)	-
Gold core Silica-dye shell (B) and TiO_2 (2)	-0.042
Gold core Silica-dye shell (B) and TiO_2 (3)	--
Silica-dye core coated in gold seeds (D) and TiO_2	-0.0185

From the results in Table 11, RhB in water and with a TiO_2 film degraded the dye resulting in a loss of fluorescence and therefore a measurable degradation rate. TiO_2 proved effective at boosting the photobleaching of RhB shown by an increase in degradation rate by a factor of x1.93. A protective element however, can be initially identified at the APS conjugation stage of which showed no loss of fluorescence. The APS was sufficient enough to protect the RhB molecule, even while undergoing UV irradiation and photocatalysis. Further coating with silica also showed no change in fluorescence as expected since additional silica within the matrix provided further protection. The SPR effect of the gold core however, provided some enhancement in photobleaching whilst in the nanoparticle structure, however, the results are not certain as one result did not fit the trend. The gold seed coating gave a similar result of a slight degradation over time. As expected the plasmons on the gold

surface enhanced photocatalysis to enable some RhB photobleaching, however, the protective properties of silica still played a large part as the rates of decay were still much smaller than when the RhB dye was without any protection, i.e. 2.7 to 0.016, this means even without photocatalytic enhancement the protective silica can decrease degradation by a factor of x174. This result however, is based on only a few tests and needs to be repeated to ensure accuracy, in particular for particle type B where the results were too erratic to provide a reliable rate of decay. This was likely due to inferior mixing during the irradiation and before testing was made causing the sample being tested to vary too much in dye concentration. Such things could be avoided by repeating the test to ensure that any change is definite and constant erratic (but small) changes could be taken as zero or a negligible change.

4. Conclusion

This project investigates the effect of plasmon boosting of TiO_2 photocatalytic films and ways this effect can possibly be enhanced through nanoparticle technology. Methods of nanoparticle synthesis were used in order to create a model for gold plasmon boosting fluorescent dye emission to be most effective. The results concluded that a silica-dye nanoparticle coated in gold seeds sized 1-3nm in diameter produced a huge increase in fluorescence compared to a silica-dye nanoparticle control by a factor of x196, or even compared to the established gold core silica-dye shell nanoparticle, which showed only the expected plasmon boosting of a fivefold increase.

TiO_2 films were fabricated by magnetron sputtering however these films only reacted to UV light so the effect of duel enhancement by both a light source and dye fluorescence emission could not be investigated. The effects of the TiO_2 films photocatalysis on the nanoparticle models was tested showing that they were capable of photobleaching RhB however they were protected once the RhB conjugated with APS. This reaction alone was sufficient at protecting the RhB molecule from being broken down, however encapsulating in silica also prevented breakdown as expected. The gold core

nanoparticle's (particle B) plasmon effects showed some effect of counteracting the protective properties of silica, however this is inconclusive. A more definitive result was found for the gold seed coated silica-dye nanoparticle (particle C), which showed a small loss of RhB over time however this was 174 times less effective than when RhB was exposed.

By using gold nanoparticles the rate of RhB breakdown was boosted by x2.13 showing that SPR does have an effect on photocatalysis. Other authors have attempted similar methods by coating the film surface with a thin layer of gold (5nm) [20], acquiring results of x66 enhancement. By using the model nanoparticle on the TiO_2 surface as explained in future work (section 4.1), it may be possible to achieve this enhancement level when exposed to UV light.

The accuracy of the results can be considered very low since few repeat results were performed to ensure any results were statistically significant. The results in this project must therefore be taken as a basic value of increase/decrease/no change in effect, whilst additional testing must be performed to provide a more accurate value.

When considering new methods of water treatment, the materials of treatment themselves must be considered. In this project silica and gold nanoparticles, rhodamine B dye and TiO_2 films were used. Silica itself is non-toxic along with gold and both are being considered for new medical treatments in the future. TiO_2 would be in the form of a static film however nanoparticle fragments could be considered a health risk since TiO_2 is a possible carcinogen [47]. Rhodamine B would also not be usable as a fluorescent molecule being classified as carcinogenic, so a different and non-toxic fluorescent molecule must be used. All these factors must be considered in case any parts of the water purification system are lost in the water itself over time. If methods of reducing this adequately are found then these factors may be bypassed.

This project has explained and verified some innovative concepts on the cutting edge of nano technology and new possibilities in the field of water purification technology, demonstrating innovative methods of utilising gold SPR and outlining a possible new system were TiO_2 photocatalysis can be enhanced in the use of effectively breaking down organic pollution of which is

a serious and growing environmental problem, which the European Union is tackling directly through the water framework directive.

.

4.1 Future Work

Several aspects of gold plasmon boosting of TiO_2 films were investigated which leads to possible new methods of plasmon boosted TiO_2. TiO_2 films can me made sensitive to visible light through doping with various elements, in particular nitrogen[45]. This can be easily achieved by introducing nitrogen gas to the magnetron sputtering chamber. The amount of nitrogen can be precisely controlled by altering the proportion of oxygen and nitrogen gas introduced. In this case nitrogen exists in ionic form (N^{3-}) with a small amount as titanium nitride (TiN). The maximum absorption can be altered to λ620nm and the band gap to 2eV[22]. This could enable the film to activate from both the gold SPR enhancement and fluorescence of encapsulated dye with a similar emission wavelength. A system could be developed to utilise visible light of which can be obtained artificially (for potentially less power than a UV lamp) or from sunlight. To maximise the potential of this system using the results from this project, nanoparticles must be fabricated to be as small as possible, be coated in a sufficient and even amount of gold seeds as possible, loaded with as much dye the maximum amount of dye without the molecules self-quenching. Finally they must be adhered to the TiO_2 film so that any SPR interactions and fluorescent emissions interact closely and efficiently with the film surface. This system will potentially break down organic molecules efficiently, for little or no artificial energy input.

References

1 **A. V. d. H. A.C. Belfroid, A.D. Vethaak, A.J. Schafer, G.B.J. Rijs, J. Wegenera, W.P. Cofinoa**, *Analysis and occurrence of estrogenic hormones and their glucuronides in surface water and waste water in The Netherlands*, ed., ed. by Editor, The Science Of the Total Environment, City, **1999**, Vol. 225, pp. 101-109.

2 **T. R. S. Jobling, R. White, M. G. Parker, J. P. Sumpter**, *A Variety of Environmentally Persistent Chemicals, Including Some Phthalate Plasticizers, Are Weakly Estrogenic* , Environmental Health Prospectus, City, **1995**, Vol. 103, pp. 582-587.

3 **H. Boyacioglu, H. Boyacioglu**, *Water pollution sources assessment by multivariate statistical methods in the Tahtali Basin, Turkey* Environ Geol **2007**, Vol. 54, pp. 275-282.

4 **R. Hites, K. Biemann**, *Water Pollution: Organic Compounds in the Charles River, Boston*, Science **1972**, Vol. *178*, pp. 158-160.

5 **European. Parliament**, *Directive of the European parliament and of the council amending Directives 2000/60/EC and 2008/105/EC as regards priority substances in the field of water policy*, European Commission, **2012**, pp. 1-31.

6 **Watts. and. Crane**, *Desk Based Review Of Current Knowledge*, Drinking Water Inspectorate, **2007**, pp. 1-107.

7 **J. C Fetzer**, *The Chemistry and Analysis of the Large Polycyclic Aromatic Hydrocarbons*". Polycyclic Aromatic Compounds, **2000,** Vol. 27, pp. 143

8 **A Luch**. *The Carcinogenic Effects of Polycyclic Aromatic Hydrocarbons*. Imperial College Press, **2005,** pp. 361-378

9 **J. Gasperia, S. Garnaud, V. Rocher, R. Moill,** *Priority pollutants in wastewater and combined sewer overflow,* Science of the Total Environment, **2008**, Vol. 407, pp. 263-272

10 **J. C. I. Espadaler, J. Om, F. Ventura, M. Cortina, F. Pauni and J. Rivera**, *Identification of Organic Pollutants In Ter River and Its System of Reservoirs Supplying Water To Barcelona (Catalonia, Spain): A Study by GC/MS and FAB/MS*, Water Research, **1997**, Vol. 31, pp. 1996-2004.

11 **Office of Water Management**, *Primer for Municipal Wastewater Treatment Systems* **2004**, 1-30.

12 **N. Water**, *http://www.pub.gov.sg/water/newater/newatertech/Pages/default.aspx*, 30/05/2013,

13 **Southern Water** *http://www.southernwater.co.uk/Environment/allAboutWater/waterTreatment/*, 30/05/2013

14 **C. V. B. Van der Bruggen**, *Removal of pollutants from surface water and groundwater by Nanofiltration: overview of possible applications in the drinking water industry,* Environmental Pollution*,* **2003**, Vol. 122, pp.435-445.

15 **S. G. J. Heijman, R. Hopman**, *Activated carbon filtration in drinking water production: model prediction and new concepts,* Colloids and Surfaces *A: Physicochemical and Engineering Aspects* **1999**, Vol. *151 pp.*, 303-310

16 **G.-S. W. H-C Lin**, *Effects of UV/H2O2 on NOM fractionation and corresponding DBPs formation,* Desalination**, 2011**, pp. 221-226.

17 **A. N. Pisarenko, D. Yana, D. Gerritya, S. A. Snydera**, *Effects of ozone and ozone/peroxide on trace organic contaminants and NDMA in drinking water and water reuse applications,* Water Research **2012**, Vol. 2, pp.316-326.

18 **T. K. L. Zhanga, N. Sanoa, A. Toyoda**, *Development of TiO2 photocatalyst reaction for water purification*, Separation and Purification Technology, **2003**, Vol. 31, pp.105-110.

19 **L. Zuwei, H. Wenbo, P. Prathamesh, A. Mehmet, C. Stephen**, *Plasmon Resonant Enhancement of Photocatalytic Water Splitting Under Visible Illumination,* Nano Letters, **2011**, Vol. 11, pp. 1111-1116.

20 **T. Ohno**, *Preparation of visible light active S-doped TiO2 Photocatalysts and their photocatalytic activities.* Water Science Technology **2004**, Vol. *49*, pp. 159-163.

21 **A. Fujishima,T. R., D. Tryk,** *Titanium Dioxide Photocatalysis*, Journal of Photochemistry and Photobiology C: Photochemistry Reviews 1 , **2000**, Vol. 1, pp.1-21.

22 **N. Serpone**, *Is the Band Gap of Pristine TiO2 Narrowed by Anion- and Cation-Doping of Titanium,* Journal of Physical Chemistry, **2006**, Vol. 110, pp.24287-24293.

23 **W. Sangchay, L. Sikong, K. Kooptarnond**, *Comparison of photocatalytic reaction of commercial P25 and synthetic TiO2-AgCl nanoparticles,* Procedia Engineering **2012**, Vol. *32*, pp. 590-596.

24 **N. Salah, M. Bouhelassa, B. David**, *Photocatalytic Decoloration of Cibacron Green RG12, on TiO2 Fixed on Mineral Supports by the PMTP Method,* Physics Procedia, **2011**, Vol. *21*, pp. 115-112.

25 **Z. Jing, Y. Song, F. Lu, W. Fei, Y. Mengqiong, L. Genxiang, X Qian, W. Xiang, L Can**, *Photocatalytic Degradation of Rhodamine B on Anatase, Rutile, and Brookite TiO2*, Chinese Journal of Catalysis **2011**, Vol. *32*, pp. 983-991.

26 **S. Ghosh, T. Pal**, *Interparticle Coupling Effect on the Surface Plasmon Resonance of Gold Nanoparticles: From Theory to Applications,* Chemical Review **2007**, Vol.*107*, pp. 4797-4862.

27 http://gregemmerich.files.wordpress.com/2012/11/lspr.jpg, 27/06/2013

28 **J. Wallace**, S*urface plasmons boost emission from dyed polymer,* Laser Focus World **2005**, pp. 36-39.

29 **S. Poznyak, D. Talapin, A. Kulak**, *Structural, Optical, and Photoelectrochemical Properties of Nanocrystalline TiO2-In2O3Composite Solids and Films Prepared by Sol-Gel Method,* Journal of Physical Chemistry **2001** , Vol. *105*, pp. 4816-4823.

30 **K. Ishii**, *High Rate Low Kinetic Energy gas-flow-sputtering System,* Journal of Vacuum Science and Technology, **1989**, Vol. *7*, pp. 256.

31 **Juan Li, Fang Mei, Wen-You Li, Xi-Wen He, Y.-K. Zhang,** *Study on the fluorescence resonance energy transfer between CdTe QDs and butyl-rhodamine B in the presence of CTMAB and its application on the detection of Hg(II)*, Spectrochimica Acta Part A, **2008**, Vol. 70, pp. 811–817.

32 **T. Yokoyama**, *Nanoparticle Technology for the Production of Functional Materials,* Kona **2005**, Vol. *25*, pp. 1-216.

33 **P. R. Lockman, R. J. Mumper, M. A. Khan, D. D. Allen**, *Nanoparticle Technology for Drug Delivery Across the Blood-Brain Barrier,* Drug Development and Industrial Pharmacy **2002**,Vol. *28*, pp. 1-13.

34 **W Stober, A Fink**, *Controlled Growth of Monodisperse Silica Spheres,* Journal of Colloid and Interface Science **1968**, Vol.*26*, pp. 62-69.

35 **A. Y. E. Mine, Y. Kobayashi, M. Konno, and L. M. Liz-Marzán**, *Direct coating of gold nanoparticles with silica by a seeded polymerization technique,* Journal of Colloidal and Interface Science, **2003**,Vol. 264, pp. 385-390.

36 **C. Graf, A. Imhof, and A. van Blaadere**n, *General Method to Coat Colloidal Particles with Silica***,** Langmuir**, 2003**, Vol. 19, pp. 6693-6700.

37 **A Vrij, A. v. Blaaderen**, *Synthesis and Characterization of Colloidal Dispersions of Fluorescent, Monodisperse Silica Spheres*, Langmuir **1992**, Vol.*8*, pp. 2921-2931.

38 **B. V. Enustun, J. Turkevich**, *coagulation of colloidal gold,* Journal of American Chemical Society, **1963**,Vol *83*, pp. 3317-3327.

39 **T. Pham, J. B. Jackson, N. J. Halas, T. R. Lee**, *Preparation and Characterisation of Gold Nanoshell Coated with Self-Assembles Monolayers*, Langmuir, **2002**, Vol. 18, pp. 4915-4920.

40 **C. Graf, A. v. Blaaderen**, *Metallodielectric Colloidal Core-Shell Particles for Photonic Applications*, Langmuir, **2002**, Vol. 18, pp. 524-534.

41 **D. Hanaor, M. Michelazzi, C. Leonelli, C. Sorrell**, *The effects of carboxylic acids on the aqueous dispersion and electrophoretic deposition of ZrO2* , Journal of The European Ceramic Society **2012**, Vol.*32*, pp. 235-244.

42 **H. C. Choi, Y. M. Chung, S. B. Kim**, *Size effects in the Raman spectra of TiO2 nanoparticles,* Vibrational Spectroscopy, **2005**, Vol. 37, pp. 33-38.

43 **H-Y. Kobauashi, T. Nakagawa, K. Gonda, M. Takeda, N. Ohuchi, A. Kasuya**, *Control of shell thickness in silica-coating of Au nanoparticles and their X-ray imaging properties*, Journal of Colloid and Interface Science, **2011**, Vol. 358, pp. 329-333

44 **O. G. Tovmachenko, C. Graf, D. J. van den Heuvel, A. van Blaaderen, H. C. Gerritsen**, *Fluorescence Enhancement by Metal-Core/Silica-Shell Nanoparticles,* Advanced Materials, **2006**, Vol. 18, pp. 91-95.

45 **S-Z Chen, P-Y Zhang, D-M Zhuang, W-P Zhu** *Investigation of nitrogen doped TiO2 photocatalytic films prepared by reactive magnetron sputtering,* Catalysis Communications, **2004**, Vol. 5, pp. 677-680.

46 **S-Z Chen, P-Y Zhang, D-M Zhuang, W-P Zhu** *Investigation of nitrogen doped TiO2 photocatalytic films prepared by reactive magnetron sputtering,* Catalysis Communications, **2004**, Vol. 5, pp. 677-680.

47 **International Agency for Research on Cancer** *Carbon Black, Titanium Dioxide, and Talc,* IARC Monographs on the Evaluation of Carcinogenic Risk to Humans, **2006**, Vol. 93, pp. 215-223